Thermodynamic Properties of Indium in Hydrothermal Ore Systems

John Nance
November 27, 2013
Advisors: Dr. Philip Candela and Dr. Philip Piccoli
Geology 394

Abstract

Indium has become an increasingly important metal over the past two decades. Indium in the form of indium tin oxide (ITO) is used as a capacitive sensor in a wide array of high-tech applications such as liquid crystal displays, light emitting diodes, touch screens, and photovoltaics. Indium is a by-product of zinc mining and the primary zinc ore mineral is sphalerite (ZnS). Sphalerite is the most important indium-bearing mineral; indium is incorporated into sphalerite by way of the coupled substitution, $Cu^{I}+In^{III}\leftrightarrow 2Zn^{II}$.

The purpose of my research is to identify the thermodynamic parameters that determine the indium concentration in hydrothermal ore systems. In an effort to determine this, I performed experiments in evacuated sealed quartz tubes. An experimental assemblage of pyrite, pyrrhotite, and indium-doped chalcopyrite and sphalerite, was loaded into a quartz tube. A strip of gold foil was placed in the center of the sulfides and LiCl-KCl salt flux is lastly loaded into the silica tube and tube sealed. The chalcopyrite and sphalerite were doped with ~7wt% roquesite ($CuInS_2$) for the starting materials. Roquesite is the indium containing component that is incorporated into sphalerite and chalcopyrite. The doping process involved taking very fine grained chalcopyrite and sphalerite, adding copper, indium, and sulfur (as the roquesite component) to the quartz tubes and running them for 5 days at 500°C. The sealed quartz tubes with the experimental charges were then placed into a vertical furnace at 500°C and experiments were performed for 5-15 days. After 5-15 days the tubes were quenched by dropping them from the furnace directly into a vat of water. The run products were extracted from the quartz tube, cleaned, and mounted on carbon tape attached to a glass slide for qualitative energy dispersive spectroscopy (EDS) analysis by the electron probe microanalyzer (EPMA). Additional run products were mounted in epoxy and polished for analysis by wavelength dispersive spectroscopy (WDS) by the EPMA. The run products were analyzed for indium concentration to identify relative changes in the indium-doped chalcopyrite and sphalerite starting materials. The gold strip was analyzed for indium, copper, and gold concentrations. Equilibrium is demonstrated by the concentration gradients in the minerals and gold being minimized and by an approach of time invariance in the results.

Two thermodynamic models were developed to deduce the relationship of the roquesite component in sphalerite to the activity of indium in a hydrothermal ore system. One model is based on experimental methods wherein sphalerite with a given roquesite mole fraction, together with other sulfides necessary to uniquely fix the activity of indium in the system, were equilibrated with gold which was used was used to sense the activity of indium in the system. The activity of indium in the gold was approximated by the mole fraction of indium in the gold, which was measured by the EPMA. The activity of indium in the gold is proportional to the mole fraction of roquesite (Xroq) in sphalerite. An activity = 0.005182 corresponds to a roquesite component of 3.3 mole percent which is a typical value from indium ores. This activity of indium in gold can then be used to estimate a hydrothermal solubility of a given Xroq in sphalerite, based on a second thermodynamic equilibrium, calculated by use of the program SUPCRT92. The above In activity and the corresponding Xroq yields a model aqueous activity of $InCl^{2+}$ on the order of $10^{-11.5}$ to 10^{-3} mol/kg, at a pH of 5.73 (neutral at 500C, 100MPa) and 3, respectively. Further, an intermediate $InCl^{2+}$ activity can be calculated at pH=3.16 that agrees with fluid inclusions observed in In ore deposits which yield1.9 to 4.1 ppm indium.

Table of Contents

Figures:

Tables:

Introduction

Indium is an important metal used in the manufacturing of indium tin oxide (ITO) which is used as a capacitive sensor in touch screens, liquid crystal displays, light emitting diodes, cell phone and laptop displays, and photovoltaic devices. The current market price of indium is near $320 per pound (October 25, 2013; www.metalprices.com). Indium tin oxide is widely used as a capacitive sensor because of its transparent and flexible properties that allow it to be easily applied to many surfaces. There are a number of substitutes being developed for ITO such as carbon nanotube coatings, graphene, and other thin film oxides (Kim et al., 2011; USGS, 2013). However, these substitutes still do not match the structural, optical, electrical properties of ITO's (Ghosh et al., 2011; Kim et al., 2011; Liu and Zeng, 2013).

The current estimate for the concentration of indium in the earth's crust is estimated to be 50-56 ppb (Rudnick and Gao, 2003; USGS, 2013). Sphalerite (ZnS) is the primary source of indium. Indium occurs only rarely in its native form, and rarely forms its own minerals; the primary production of indium is as a by-product of zinc refinement from sphalerite-bearing ores. Indium behaves as a chalcophile element along with many other elements such as lead, silver, zinc, arsenic, and tin, which are often found in association with sulfide deposits (Goldschmidt, 1937). Given that indium is trivalent and zinc is divalent, indium must be incorporated into sphalerite by way of a coupled substitution with copper ($Cu^{I}+In^{III}\leftrightarrow 2Zn^{II}$) or other univalent chalcophile elements of appropriate radius (Johan, 1988). A limited solid solution between sphalerite (ZnS) and roquesite ($CuInS_2$) has been suggested (Burke and Kieft, 1980; Oen et al., 1980) and was demonstrated in my experiments from Geology 393.

Indium is found in many different types of ore deposits. These include granite associated vein-stockwork, volcanogenic massive sulfide (VMS), Cornwall-type tin, Mississippi-Valley-type, porphyry copper, epithermal, sediment-hosted (SEDEX), and skarn deposits. The primary indium bearing zinc-ores are associated with hydrothermal vein-type and volcanogenic massive sulfide type deposits (Schwarz-Schampera and Herzig, 2002). To this end I researched the hydrothermal fluid thermodynamics of the indium-bearing system.

Average concentrations of indium in sphalerite range from approximately 0 to 1900 ppm (Table 1) in vein-type deposits from Canada, Japan, Bolivia, and China (Murakami and Ishihara, 2013). Three significant mines, Toyoha, Huari Huari, and Mount Pleasant, had maximum indium concentrations in sphalerite of 1,030, 3,080, and 12,500 ppm, respectively (Murakami and Ishihara, 2013). These sphalerite minerals also formed at or above 400°C, suggesting that temperature does have an effect on the maximum indium concentration in sphalerite.

Vein-type deposits are generally associated with granite and occur in the first few km of the earth's crust. The veins form as hydrothermal fluids flow through fractures or other spaces in the host rock. The minerals are then precipitated from the fluid to form the veins. Mineral assemblages of sphalerite, pyrrhotite, pyrite, chalcopyrite, galena, cassiterite and molybdenite are common (Boorman and Abbott, 1967). Fluid inclusions in sphalerite indicate formation temperatures ranging from 200° to 421°C (Fryklund and Fletcher, 1956; Shikazono and Shimizu, 1992; Murakami and Ishihara, 2013). Similar homogenization temperatures were also observed in quartz inclusions from indium-bearing ore deposits (Zhang, 2007). Mount Pleasant is a vein-stockwork tin deposit that exhibits a 1.25 wt% indium in sphalerite. In the Gasborn area, Sweden, sphalerite from skarn deposits was found to have indium concentrations ranging from less than 0.05 to 15 wt% (Kieft and Damman, 1990).

Volcanogenic massive sulfide deposits form at or near the seafloor as lenses of sulfide.

These deposits are formed by precipitation of sulfides from hydrothermal fluids associated with seafloor convection (Galley et al., 2007). VMS deposits are formed in extensional tectonic settings (Galley et al., 2007). Over 800 VMS deposits are known worldwide (Galley et al. 2007). They are commonly rich in Zn, Cu, Pb, Ag, and Au (Galley et al., 2007). Typical formation temperatures for massive sulfide deposits range from 300 to 400°C (Franklin et al., 2005). Homogenization temperatures in sphalerite in the VMS deposit at Gacun, China were around 250°C (Hou et al., 2001). The Neves-Corvo mine is a volcanogenic massive sulfide deposit with up to 54,500 ppm indium in sphalerite (Table 1).

In Geology 393 my hypothesis was that the maximum indium concentration in sphalerite reported in the literature at a given formation temperature, represents the maximum permitted at the given temperature and fugacity of sulfur. I found no apparent maximum concentration of indium in sphalerite at 500°C up to 23 weight percent and 8.5 weight percent in chalcopyrite. These values are beyond any found in natural ores. These data are not consistent with my hypothesis Further, there is at least an extensive partial solid solution between $CuInS_2$ and ZnS that extends beyond indium concentrations found in ores. Table 1 shows the maximum indium concentrations observed in those experiments. Appendix II includes all of the EPMA data from those experiments. Appendix III includes the BSE images of the run products showing compositional variability and textures.

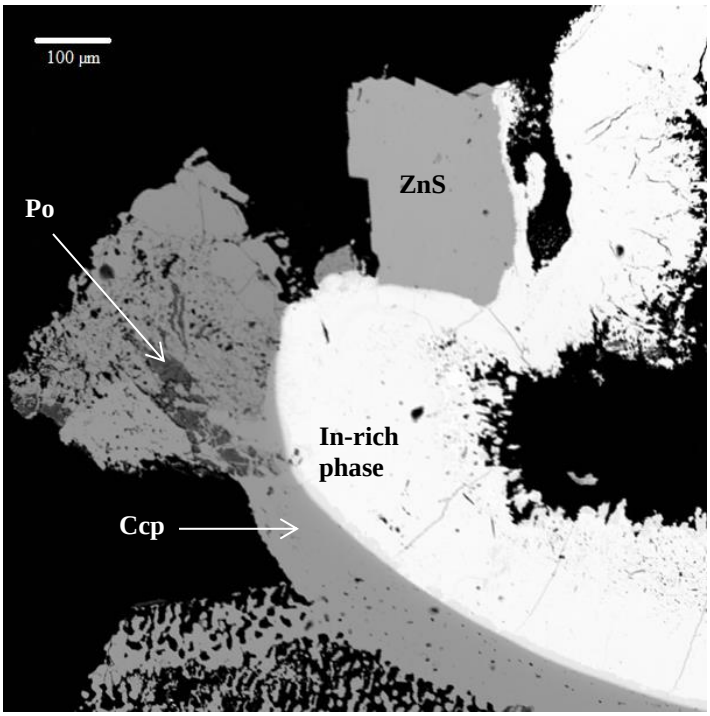

(Figure 1) Experiment 1 - Grain 3. Indium rich core, copper rich rim. Chalcopyrite, pyrrhotite, and sphalerite present.

Mineral	Maximum Indium (wt %)
Pyrrhotite	0.0521
Pyrite	0.0074
Chalcopyrite	8.5
Sphalerite	23

(Table 1) Maximum indium concentrations observed in mineral phases present.

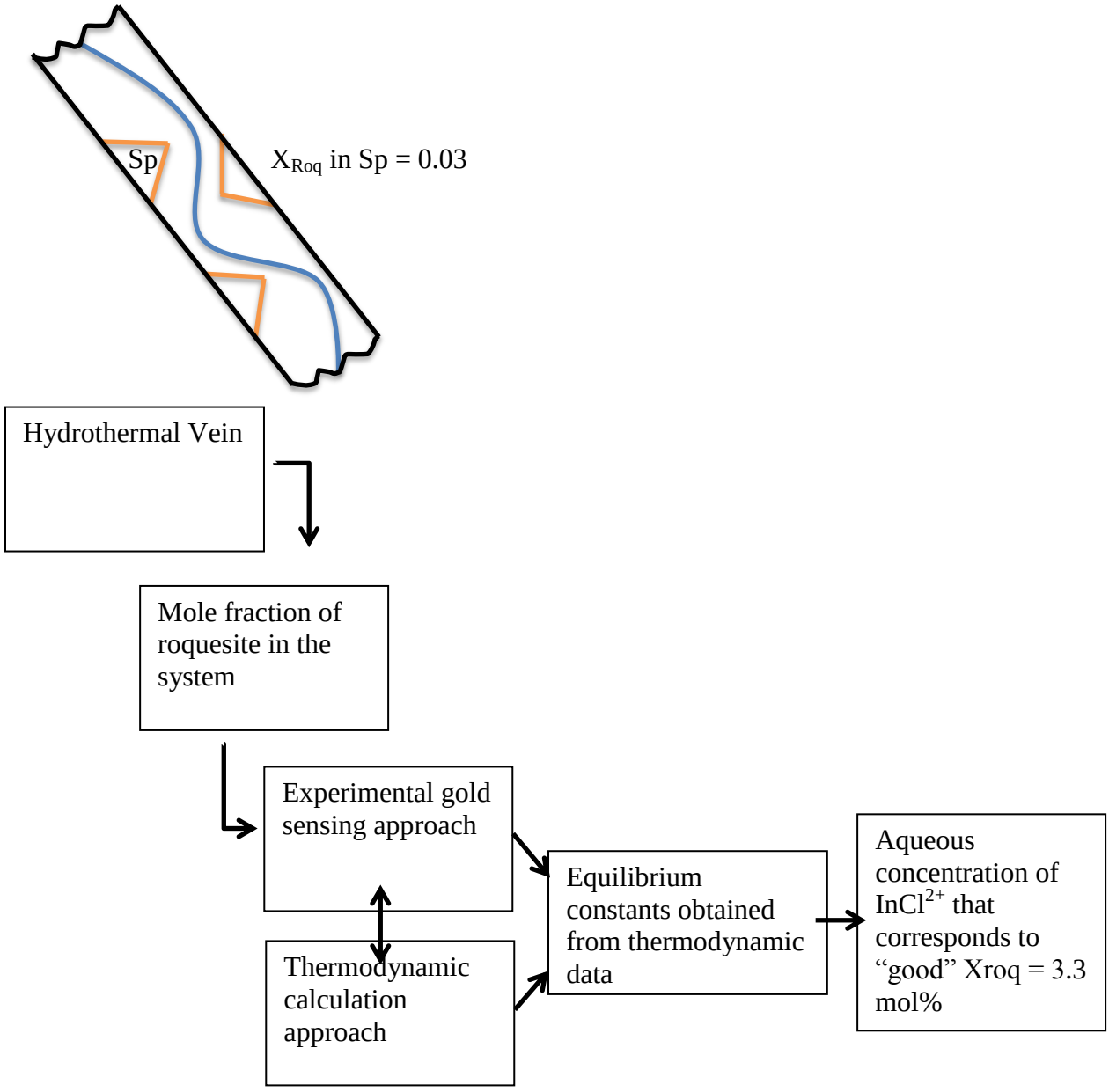

(Figure 2) Figure showing order of processes.

Figure 2 is a flow diagram that demonstrates the order of processes taken in this research. Everything starts with a hydrothermal vein deposit of interest with crystallizing sphalerite and X_{Roq} in sphalerite = 0.03. In order to make sense of the Xroq in the system two models were developed. One determines the activity of indium in the system by using the gold sensor method. The other is solely based on thermodynamic data. These models both yield an activity of indium in the system. That activity is then used in equilibrium constant equations to determine a model $InCl^{2+}$ concentration of an ore-forming hydrothermal vein.

Hypotheses

The aim of my research in Geology 394 was to determine the relationship between the indium content of ore minerals and the activity of indium in an ore-forming system, i.e. hydrothermal fluids. Further, this can be used to calculate a model hydrothermal concentration of indium in ore-forming solutions.

My hypothesis is that the activity of indium as determined by an Au-Cu-In solid solution sensor in experiments with roquesite-bearing sphalerite will yield model hydrothermal concentrations of indium that correspond to those found in fluid inclusions. The associated model that relates Xroq to thermodynamic parameters in ore-forming systems can inform explorationists regarding the possible exploration guides to finding In ores (e.g., how fO2, magmatic fractionation, and pH can affect ore formation).

Experimental Design

In Geology 393 I performed experiments in evacuated, sealed quartz tubes. The starting materials include pyrite (FeS_2), pyrrhotite ($Fe_{1-x}S$), sphalerite (ZnS) and chalcopyrite ($CuFeS_2$) along with indium metal (99.9%), and sulfur (lab grade). These components are mixed in molar proportions given by the stoichiometric coefficients in the equilibria (insert equil here). A LiCl-KCl salt flux is added in a 1:1 ratio by volume to the other starting materials. The starting materials are mixed thoroughly to promote homogeneity. Table 2 lists the starting materials and the weights of each material added.

Run	Starting Material (mg)								Duration	Grain size
	Ccp	Py	Po	Sp	In	Zn	S	KCl-LiCl	hours (days)	
#1	0.1606	0.0525	0.0381	0.0851	0.1039		0.0428		168 (7)	$\leq$ 1 mm
#2	0.1607	0.0549	0.0390	0.0848	0.1004		0.0415	0.20	163 (~7)	~50 µm
#3	0.1607	0.0536	0.0385	0.0856	0.1002		0.0425	0.18	163 (~7)	~50 µm
#4	0.1601	0.0530	0.0399		0.1033	0.0562	0.0702	0.20	331 (~14)	~50 µm
#5	0.1598	0.0525	0.0404		0.0996	0.0560	0.0701	0.18	331 (~14)	~50 µm
#6	0.0126	0.0082	0.0060	0.0067				0.02	120 (5)	~50 µm
#7	0.0112	0.0079	0.0064	0.0069				0.02	120 (5)	~50 µm
#8	0.0114	0.0078	0.0053	0.0069				0.02	240 (10)	~50 µm
#9	0.0116	0.0079	0.0056	0.0069				0.02	240 (10)	~50 µm
#10	0.0122	0.0081	0.0060	0.0060				0.02	360 (15)	~50 µm
#11	0.0121	0.0078	0.0054	0.0066				0.02	360 (15)	~50 µm

(Table 2) Starting materials from all experiments

(Figure 3) Images showing the evacuated sealed quartz tube being made and the final sealed quartz tube. The open end of the tube is attached to a vacuum and the tube is held in the flame to melt and seal it. (Images courtesy of Michael Mengason).

Quartz tubing from Technical Glass© is used in this project (ID = 5 mm, OD = 7 mm) for experiments 1-5. For experiments 6-11 Heraeus Quarzglas (ID = 2 mm, OD = 7) is used. The quartz tubing was changed from thin wall to thick wall because of experiment failures experienced at the beginning of the semester. One end of the quartz tube is sealed by the use of an oxygen-methane flame (Figure 3). The experimental assemblage is then loaded (Figure 4) into the empty quartz tube. Lithium chloride and potassium chloride are added on top of the other starting materials. The salt is added to catalyze the reaction by (variably) dissolving reactants and transporting them to sites of reactions at mineral grain surfaces; this occurs by diffusion through the molten salt itself. The addition of salt does not promote diffusion through the minerals though, so that problem is solved only by reducing the diffusion distance (i.e. reducing the radius

of the grains), and by extending the run time. The quartz tube containing the starting materials is then placed under vacuum and the remaining open end is sealed with an oxygen-methane flame (Figure 3). The sealed quartz tubes are photographed and sketched for identification. Heat resistant chromel wire is wrapped around the tube and affixed to a thermocouple. The tube and thermocouple are then lowered into a vertical furnace (Figure 6) that has been heated to the desired temperature; 500˚C in this case. The temperature gradient over the sample has been estimated to be 1-3˚C.The experiments are then run for 5 to 15 days. At the end of the specified time, the experiments are quenched in room temperature water.

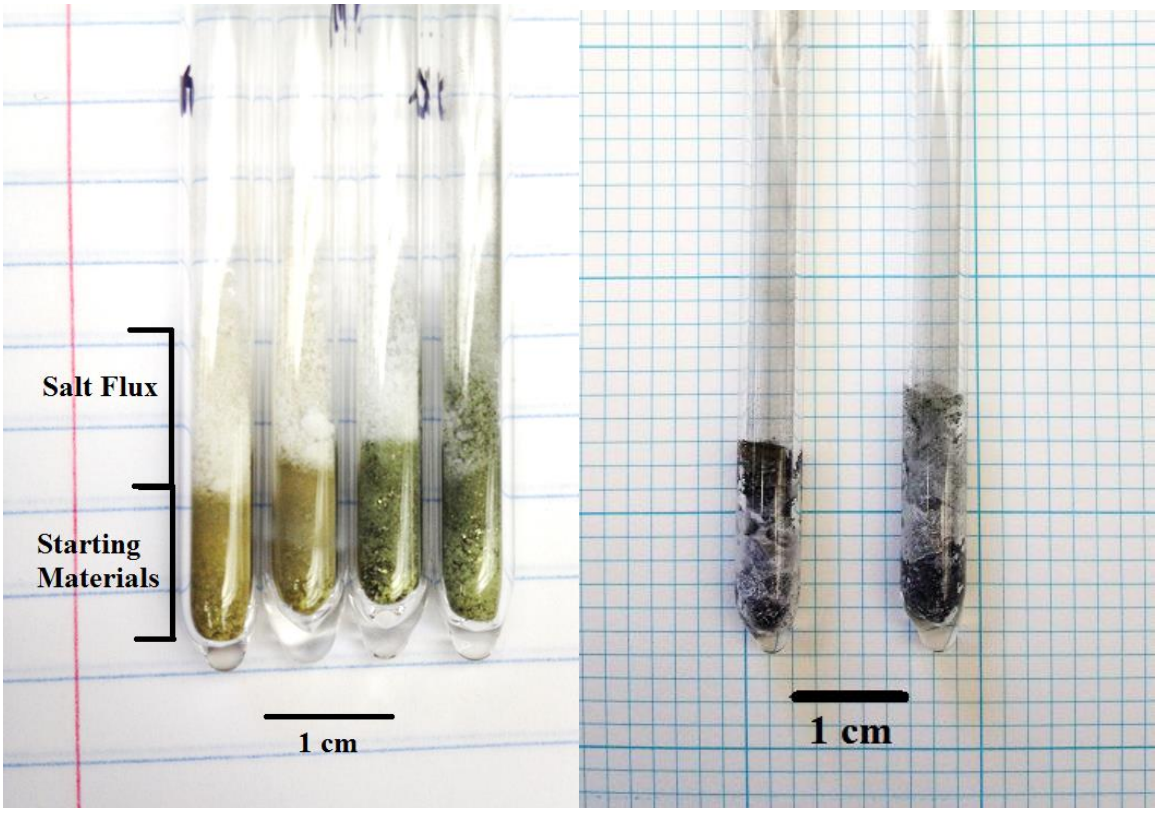

(Figures 4-5) Figure 4 (left) depicts the quartz tubes loaded with starting materials and salt flux. Figure 5 (right) shows the sealed quartz tubes from experiment 2 and 4 after being quenched.

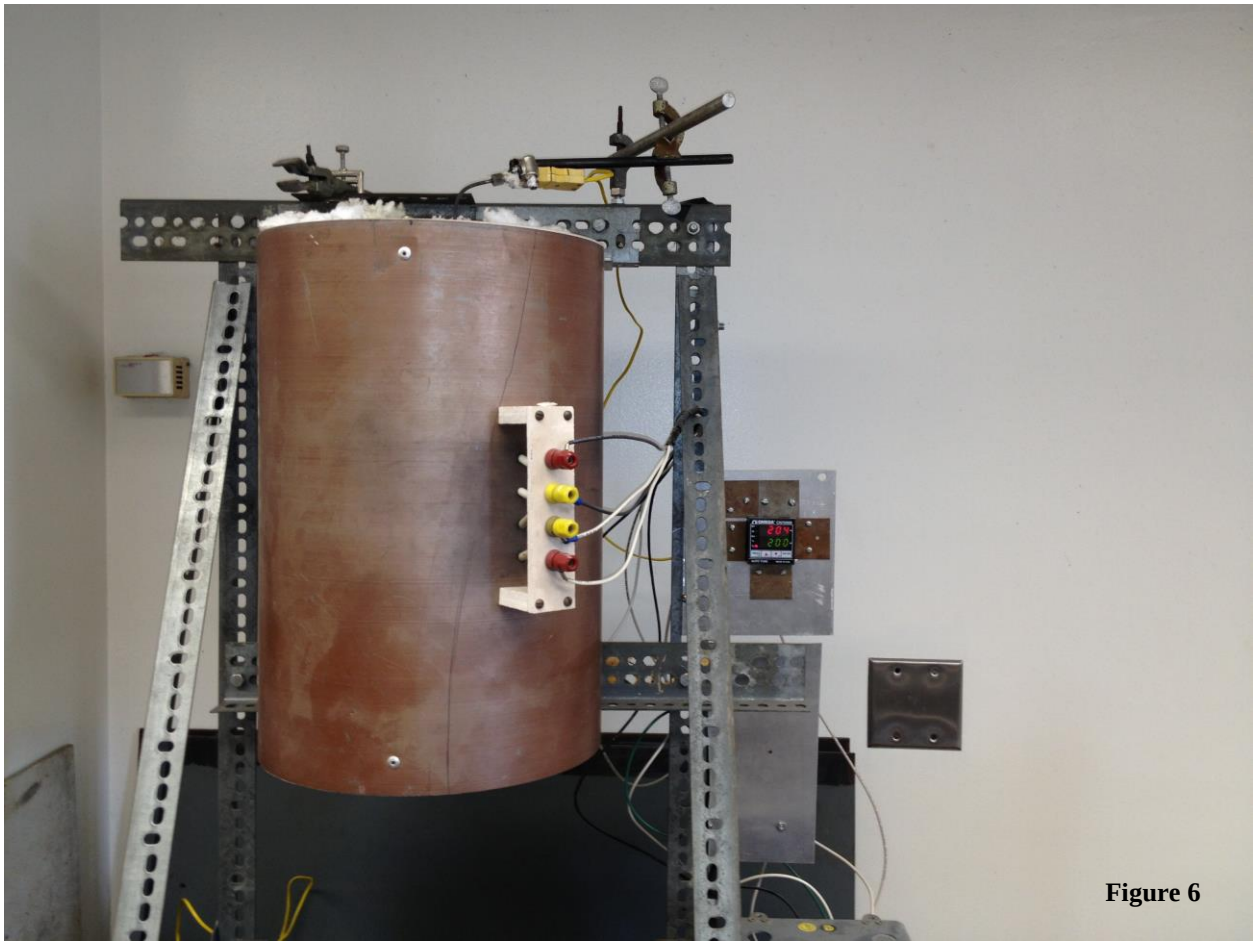

(**Figure 6)** Vertical furnace used in experiments with thermocouple at the top, temperature controller to the right and heating element wires on the furnace face.

After the experiments have been quenched (Figure 5), the sealed quartz tubes are opened by scoring the quartz tube and snapping it open. The run products are extracted from the tube and placed in a glass funnel lined with filter paper. The run products are cleaned using distilled water and then acetone to inhibit oxidation. The cleaned run products are placed in vials until they are ready to be set in epoxy mounts.

The grains are affixed to the base of a plastic mold (Figure 7) with double sided tape. The epoxy, Buehler© EpoFix, is mixed with the hardener according to a 15:2 ratio (by volume). The epoxy/hardener is mixed vigorously for 5 minutes. The epoxy is then slowly poured into the plastic mold and allowed to cure for at least 24 hours. Once cured the epoxy mounts are removed from the mold.

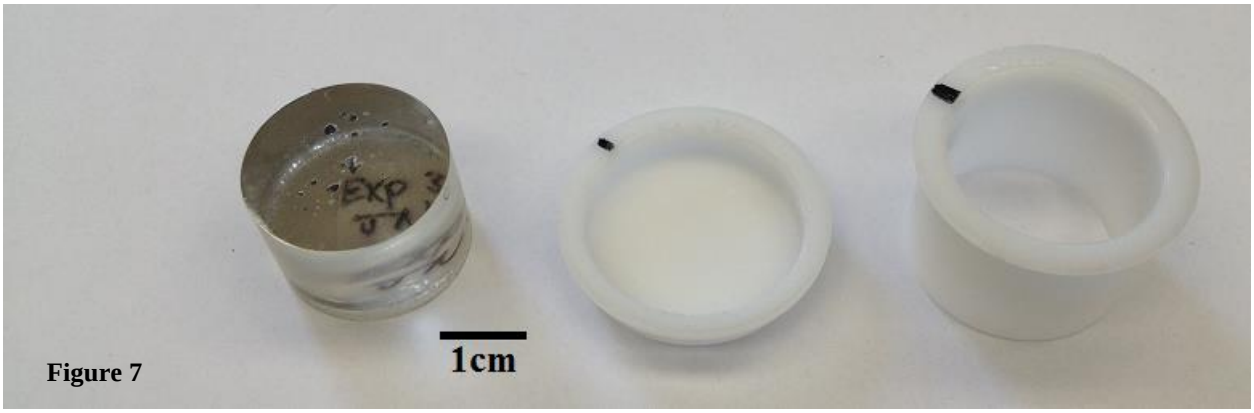

Figure 7

(Figure 7) From left to right: polished and carbon coated epoxy mount, mold base, and mold sleeve. A paper label is embedded in the mount.

Sand paper of varying grit sizes is used to roughly polish the epoxy. Finer and finer grits were used to smooth the surface. The mount is washed with soap and water between grit sizes to prevent contamination. Buehler© diamond paste is used to continue the polishing process. A 9 micron and 3 micron paste are used on paper with mineral oil to obtain a glassy surface. A 0.1 micron alumina suspension is used with a felt pad to get the finest polish and to remove scratches. The mounts are set in a beaker with distilled water and placed in an ultrasonic bath to remove any residual polish that may interfere with analyses.

The overall design of the experiments remained the same from Geology 393 and Geology 394. The primary change was in the phases used in each experiment. I redesigned my experimental setup in order to facilitate the calculation of the activity of indium in the system of interest (In-Cu-Fe-S-Zn), to include the minerals pyrite, pyrrhotite, chalcopyrite, and sphalerite. I synthesized new starting materials with a known roquesite component (i.e., ~7 wt % indium in chalcopyrite and sphalerite which is on the order of the maximum found in naturally occurring deposits).

By using starting materials with a known indium concentration, I was able to monitor the change in indium content of the minerals in the system of interest. Chalcopyrite and sphalerite were loaded into separate quartz tubes with a salt flux and elemental copper, sulfur, and indium in proportion to form the ~7wt% roquesite component doped starting materials. The first attempt at these syntheses resulted in the explosion of the quartz tubes because the salt flux is hygroscopic and water was introduced into the system. Pressure built in the tube and exceeded the strength of the quartz tube. This set me back by about 2 weeks. The second attempt resulted in successful runs. The EDS analyses of the run products showed that indium-bearing starting materials were in fact synthesized.

After completing the synthesis of the new starting materials, I ran a new series of experiments for the system of interest. Pyrite, pyrrhotite, and indium-doped chalcopyrite and sphalerite were placed into a quartz tube. A small strip of gold foil was inserted into the center of the sulfide mixture extending the full length of the sulfides. Finally the salt flux was added to the quartz tubes. Multiple such tubes were prepared. The tubes were evacuated, sealed and placed in a vertical furnace for 5 to 15 days at 500°C. Approach toward equilibrium was demonstrated by the minimization of concentration gradients among the minerals and within the gold strip and by an approach of time invariance in the results.

Thermodynamic Models

The Zn-In-Cu-Fe-S system is complex. I present two thermodynamic models for calculating the activity and concentration of indium in an ore forming system. First I present the thermodynamic model for calculating activity of indium in an ore forming system. Second I present an experimental model for calculating the activity of indium in my experimental system. This second model utilizes a novel gold sensing technique and presents the steps for calculating the activity of indium in my experiments, which can then serve as input to the calculation of hydrothermal concentrations that correspond to the indium concentrations of the phases in my quartz tube experiments.

In the thermodynamic model used to calculate the activity of indium in the system I utilized the following sources to calculate the thermodynamic data. SUPCRT92 is software designed to calculate thermodynamic properties of minerals over a range of temperatures (0 to 1000°C) and pressures (1 to 5000 bar) (Johnson et al., 1992). SUPCRT92 has been used to calculate free energy and equilibrium constants (Table 3) in portions of the experimental system (Johnson et al., 1992). However, the data on indium-bearing phases in SUPCRT92 is incomplete and therefore data for the roquesite component in sphalerite had to be taken from Migge and Grzanna (1993) and data for indium metal, from F*A*C*T (http://www.crct.polymtl.ca/fact/index.php) had to be incorporated into the calculations.

Important Basic Equations

The Gibbs free energy for a solid solution containing Cu, In, and Au is given by equation 1. This is the mole fraction weighted sum of the chemical potential of each component:

$$\Delta\overline{G}_f^{\circ} = x_{Cu}\mu_{Cu} + x_{In}\mu_{In} + x_{Au}\mu_{Au} \qquad \textbf{Eq. 1}$$

where x_i is the mole fraction of each component, and μ_i is the chemical potential of each component. The chemical potential, which is a measure of the reactivity of a component, is given by:

$$\mu_i = \Delta\overline{G}_f^{\circ} + RTlna_i, \qquad \textbf{Eq. 2}$$

where $\Delta\overline{G}_f^{\circ}$ is the Gibbs free energy of formation, **R** is the ideal gas constant 8.314 J/mol-K**, T** is temperature in Kelvin and a_i is the activity.

Equation 2 can also be written as:

$$\mu_i = \Delta\overline{G}_f^{\circ} + RTln_{x_i} + RTln_{\gamma_i} \qquad \textbf{Eq. 3}$$

where γ_i is the activity coefficient.

The Gibbs free energy of formation is a measure of the stability of the pure component relative to the elements at 25°C and 1 bar. The $RTln_{xi}$ term accounts implicitly for the ideal entropy of mixing and the activity coefficient accounts for the interactions that occur between the components in the mixture above and beyond the simple mixing account for in the second term of equation 3.

For an example of mixing between two components, consider a carton of eggs. The end members are brown eggs and white eggs (6 each) in an egg carton. The ln_x term accounts for the various ways that those eggs can be arranged in the carton. The ln_γ (activity coefficient) accounts for the molecular interactions beyond the simple mixing of the eggs. This includes the electrical and quantum interactions that occur in a mixture beyond the statistical mixing of atoms modeled by the white and brown egg analogy.

Equation 4 is the result of combining equations 1 and 3. This new equation defines the Gibbs free energy of the ternary system; Au, Cu, In.

$$\Delta\overline{G}_f^{\circ} = (x_{Cu}\mu_{Cu} + x_{In}\mu_{In} + x_{Au}\mu_{Au}) + \left(x_{Cu}RTln_{x_{Cu}} + x_{In}RTln_{x_{In}} + x_{Au}RTln_{x_{Au}}\right) + (x_{Cu}RTln_{\gamma_{Cu}} + x_{In}RTln_{\gamma_{In}} + x_{Au}RTln_{\gamma_{Au}}) \quad \textbf{Eq. 4}$$

The first parenthetical term of this equation is the mole fraction weighted sum of the thermodynamic properties of the end members. The second gives the thermodynamic properties of the ideal mixture, and the third is the excess free energy of mixing ($\bar{G}^{ex}$) which describes the thermodynamics of non-ideality. If one has data on the third term from the literature, one can in principle, extract an activity coefficient for indium in the gold foil. This could then be combined with a mole fraction of indium, in gold foil from my experiments, to obtain an activity of indium from my experiments. These parts will be discussed in more depth below and I present a way to combine constituent binary systems (Au-In, Cu-In, Au-Cu) into the ternary Au-In-Cu system.

Thermodynamic Data Model

Here I present an alternative method for calculating the activity of indium in the system. The chemical potentials of the phase components in the system (Cu-In-Zn-S-Fe) can be written in terms of the chemical potentials of the system components. For example the chemical potential of the roquesite phase component in the sphalerite can be written in terms of the chemical potentials Cu, In, S_2 in the system:

$$\mu_{CuInS_2} = \mu_{Cu} + \mu_{S_2} + \mu_{In}. \quad \textbf{Eq. 5a}$$

The chemical potentials of the other phase components in the experimental system can be similarly written.

$$\mu_{CuFeS_2} = \mu_{Cu} + \mu_{S_2} + \mu_{Fe}, \quad \textbf{Eq. 5b}$$

$$\mu_{FeS_2} = \mu_{Fe} + \mu_{S_2}, \quad \textbf{Eq. 5c}$$

$$\mu_{FeS} = \mu_{Fe} + \frac{1}{2}\mu_{S_2}, \quad \textbf{Eq. 5d}$$

$$\mu_{Fe_2S_3} = \mu_{Fe_2} + \frac{3}{2}\mu_{S_2}, \quad \textbf{Eq. 5e}$$

$$\mu_{ZnS} = \mu_{Zn} + \frac{1}{2}\mu_{S_2}. \quad \textbf{Eq. 5f}$$

Pyrrhotite, with a nominal composition of $Fe_{1-x}S$, is a solid solution of the two phase components, FeS and Fe_2S_3.

The individual chemical potentials of the system components Cu, In, and S_2, can be represented by the equations 6, 7, 8, respectively:

$$\mu_{Cu} = CuFeS_2 - FeS_2, \quad \textbf{Eq. 6}$$

$$\mu_{In}\ is\ a\ function\ of\ the\ a_{In}\ in\ gold\ foil, \quad \textbf{Eq. 7}$$

$$\mu_{S_2} = 2FeS_2 - 2FeS. \qquad \text{Eq. 8}$$

The equations above (6-8) can be derived for each of equations: 5a-5f. The activity of indium in the Au-Cu-In alloy is equal to the mole fraction of indium times its activity coefficient. If we substitute equations 6 and 8 into equation 5a, equation 9 results:

$$\mathbf{FeS_2 + In + CuFeS_2 = 2FeS + CuInS_2} \qquad \text{Eq. 9}$$

A balanced chemical reaction is really a relationship among chemical potentials of the phase components as well as a statement of equilibrium. If we take equation 2 and integrate it into equation 9 we get equation 10:

$$RTlna_{FeS}^2 + RTlna_{CuInS_2} - RTlna_{CuFeS_2} - RTlna_{FeS_2} - RTlna_{In} = \Delta\overline{G}^{\circ}_{fCuInS_2} + 2\Delta\overline{G}^{\circ}_{fFeS} - \Delta\overline{G}^{\circ}_{fCuFeS_2} - \Delta\overline{G}^{\circ}_{fFeS_2} - \Delta\overline{G}^{\circ}_{fIn} \qquad \text{Eq. 10}$$

Equation 10 can be reduced and written more precisely by using the rules for adding logarithms on the left, and the right written as a sum:

$$-RTln\frac{a_{FeS}^2 * a_{CuInS_2}}{a_{CuFeS_2} * a_{FeS_2} * a_{In}} = \sum \nu_i * \Delta\overline{G}^{\circ}_f \qquad \text{Eq. 11}$$

where **ν**, the stoichiometric coefficients, are by convention, positive for products, negative for reactants.

$$-RTlnK = \sum \nu_i * \Delta\overline{G}^{\circ}_f \qquad \text{Eq. 12}$$

where K, the equilibrium constant, and is defined by:

$$K = \frac{a_{FeS}^2 * a_{CuInS_2}}{a_{CuFeS_2} * a_{FeS_2} * a_{In}} = \frac{x_{FeS}^2\gamma_{FeS}^2 * x_{CuInS_2}\gamma_{CuInS_2}}{x_{CuFeS_2}\gamma_{CuFeS_2} * x_{FeS_2}\gamma_{FeS_2} * x_{In}\gamma_{In}}. \qquad \text{Eq. 13}$$

Equilibrium Constants

This equilibrium constant shows that the activity of indium in the foil, in my experiments, is a measure of the chemical potential of indium in the experimental system, as expressed by the roquesite mole fraction in sphalerite, which was chosen to represent the mole fraction of roquesite in ores such as that found at Toyoha. The activity of indium in the foil contains, implicitly, all the activities and the equilibrium constant. Alternatively, one can calculate the K from free energy data (Eq. 12). One can then enter plausible activities for sulfide phase components based on the composition of the phases in ores, and calculated an estimated activity of indium in foil. In either case, the measured or calculated indium activity, both reflecting reasonable order of magnitude roquesite mole fractions from ores, can be used as input to the following equilibrium for a model hydrothermal ore fluid:

Equilibrium: $\mathbf{In^{metal} + 0.75O_2 + 3H^+ + Cl^- = InCl^{2+} + 1.5H_2O}$ **Eq. 14**

Component(s)	ΔG_f (Joule/mole)	Source
$\mathbf{0.75O_2 + 3H^+ + Cl^- = InCl^{2+} + 1.5H_2O}$	-473855	SUPCRT
$\mathbf{FeS_2 + CuFeS_2 = 2FeS}$	183811	SUPCRT
$\mathbf{CuInS_2}$	-264587	Migge, 1993
$\mathbf{In^{metal}}$	-37538	F*A*C*T

(Table 3) Components used to calculate the equilibrium constants for the two equilibria in equations 9 and 14.

By using equation 12 and using data from SUPCRT, F*A*C*T, and Migge (1993) in table 3 the following equilibrium constants were obtained:

$K_{Eq.9} = 10^{2.92}$ for equation 9
$K_{Eq.14} = 10^{29.48}$ for equation 14

Applying equation 13 to each equilibria in equations 9 and 14 results in equations 15 and 16, respectively:

$$\mathbf{K_{Eq.9} = 10^{2.92}} = \frac{a^2_{FeS} * a_{CuInS_2}}{a_{CuFeS_2} * a_{FeS_2} * a^{foil}_{In}}, \qquad \textbf{Eq. 15}$$

$$\mathbf{K_{Eq.14} = 10^{29.48}} = \frac{f_{H_2O}{}^{1.5} * a_{InCl^{2+}}}{f_{O_2}{}^{0.75} * a_{H^+}{}^3 * a_{Cl^-} * a^{foil}_{In}}. \qquad \textbf{Eq. 16}$$

The relationship of indium and indium chloride is expressed in the equilibrium from equation 13. In order to create a balanced equilibrium H^+ and thus pH is inherently involved in the equation. At 500°C and 1000 bar, log K_w = -11.463, dividing by 2 gives a pH of -5.73 which is the neutral pH at the given temperature and pressure. The log K_w is the equilibrium constant for water.

a_{Cl-}	=	1 molal (at 5.73 pH) and 3 molal (at 3 pH)
f_{H2O}	=	478 – can be estimated from the fugacity of H_2O
a^2_{FeS}	=	1 – approximately 1 from Toulmin and Barton (1963)
a_{FeS2}	=	1 – pure mineral phase
f_{O2}	=	10^{-25} – can be estimated from the fugacity of $O_{2\ –\ based}$ on FMQ from MORB
a_{H+}	=	$10^{-5.73}$ – pH is an effective activity of hydrogen activity
a_{CuFeS2}	=	1 - pure mineral phase

(Table 4)

			Activity InCl (mol/kg)	
	Xroq in sp	**Activity In in metal**	**Nuetral (pH = 5.73)**	**Acidic (pH = 3)**
$\mathbf{X^{Sp}_{Roq} = 0.00011}$	expt 0.03	0.005182	3.76E-12	0.001747
$\mathbf{X^{Ccp}_{Roq} = 0.0257}$	calc 0.01	0.000012	8.72E-15	0.000004
$\mathbf{X^{Metal}_{In} = 0.000019}$	calc 0.03	0.000036	2.62E-14	0.000012
	calc 0.06	0.000072	5.23E-14	0.000024

(Table 5) Calculated activities and mole fractions from the experiment and thermodynamic model

Thermodynamic Model using Gold Sensor Method

The equilibrium activity of indium metal (In^o) in the experiments was sensed by placing a gold strip in the sulfide mixtures. Calculation of the activity of indium from the mole fraction can be problematic. This requires the estimation of the molar excess free energy ($\bar{G}^{ex}$) of mixing

of a ternary In-Au-Cu alloy, from which an activity coefficient for indium can be calculated. The thermodynamic mixing parameters can be estimated for the ternary system from the excess functions for the constituent binaries: In-Cu, In-Au, Au-Cu.

The third term in equation 4, $\bar{G}^{ex}$, can be determined for the constituent binaries of the system. The excess free energy equations for the constituent binaries are given below (eq. 17, 19, 20).

The excess free energy ($\bar{G}^{ex}$) for the In-Cu binary (Liu et al., 2002) is given by:

$$\bar{G}^{ex}_{Cu,In} = x_{Cu} * x_{In}[L^0(x_{Cu} - x_{In})^0 + L^1(x_{Cu} - x_{In})^1 + L^2(x_{Cu} - x_{In})^2] \quad \text{Eq. 17}$$

where x_{Cu} and x_{In} are the mole fractions of Cu and In in the phase respectively, and the L values are temperature dependent coefficients given by:
L^0 = -6475.9 + 21.830T,
L^1 = -29935.2 – 5.672T,
L^2 = 47350.2 – 40.210T.

A phase diagram is a map of the thermodynamic properties of coexisting phases on the a given plane, in this case the (T,x) plane. The L values are extracted from compositional data on the equilibrium (tie line) between phases as represented by the phase diagram for the system. They are a mathematical representation of the excess free energy and the excess free energy is a mathematical manipulation of the activity coefficient. Equation 19 is used to statistically determine each optimized L value.

$$\mu^{fcc}_{In} + RTlnx_{In} + x_{Au}x_{In}L^{fcc}(x_{Au} - x_{In}) = \mu^{liq}_{In} + RTlnx_{In} + x_{Au}x_{In}L^{liq}(x_{Au} - x_{In}) \quad \text{Eq. 18}$$

The excess free energy ($\bar{G}^{ex}$) for the In-Au binary (Liu et al., 2003) is given by:

$$\bar{G}^{ex}_{In,Au} = x_{Au} * x_{In}[L^0(x_{Au} - x_{In})^0 + L^1(x_{Au} - x_{In})^1] \quad \text{Eq. 19}$$

where x_{Au} and x_{In} are the mole fractions of Au and In in the phase, and
L^0 = -48493.65 + 46.6237T – 68308T*ln(T),
L^1 = 498.45.

Similarly, the excess free energy ($\bar{G}^{ex}$) for the Au-Cu binary (Sundman et al., 1998) is given by:

$$\bar{G}^{ex}_{Au,Cu} = x_{Au} * x_{Cu}[L^0(x_{Au} - x_{Cu})^0 + L^1(x_{Au} - x_{Cu})^1], \quad \text{Eq.20}$$

where x_{Au} and x_{Cu} are the mole fractions of Au and Cu in the phase, and
L^0 = -28000 +78.8T – 10T∗ln(T),
L^1 = 6000.

Calculation of Ternary Thermodynamic Properties from the Constituent Binaries

Following the method of Chou (1995), the ($\bar{G}^{ex}$) for the constituent binaries can be combined into an estimate of the excess function for the ternary by using the equation

$$\bar{G}^{ex}_{In,Au,Cu} = Y_{In,Au} * \bar{G}^{ex}_{In,Au} + Y_{Cu,In} * \bar{G}^{ex}_{In,Cu} + Y_{Au,Cu} * \bar{G}^{ex}_{Au,Cu} \quad \text{Eq. 21}$$

where

$Y_{ij} = \frac{x_i x_j}{X_{i(ij)} X_{j(ij)}}$.		**Eq. 22**

$\bar{G}^{ex}_{In,Au,Cu}$ and $\bar{G}^{ex}_{In,Au}$ represent the ternary and binary molar excess free energies of mixing respectively, and Y_{ij} is the weighted probability as defined by equation 22, and where $X_{i(ij)}X_{j(ij)}$ represent the compositions in the indicated binaries. The variables x_i and x_j represent the mole fraction of components in a ternary system.

As stated above, the activity of indium in the Au-Cu-In alloy is equal to mole fraction of indium times the activity coefficient. The activity coefficient can be calculated from the excess free energies of mixing equations. Therefor the activity of indium metal, as obtained from the gold foil, can be used to infer the concentration of indium in hydrothermal aqueous solution. This was then compared to indium concentration observed in fluid inclusions (Zhang et al, 2007). The calculated activity of indium was used in conjunction with SUPCRT92, to get model estimates of indium solubility in hydrothermal ore fluids.

The calculations were performed at 500°C which makes the thermodynamics simpler because at this temperature the putative face-centered cubic phases in the constituent binaries are disordered, and their thermodynamic excess functions are therefore much simpler.

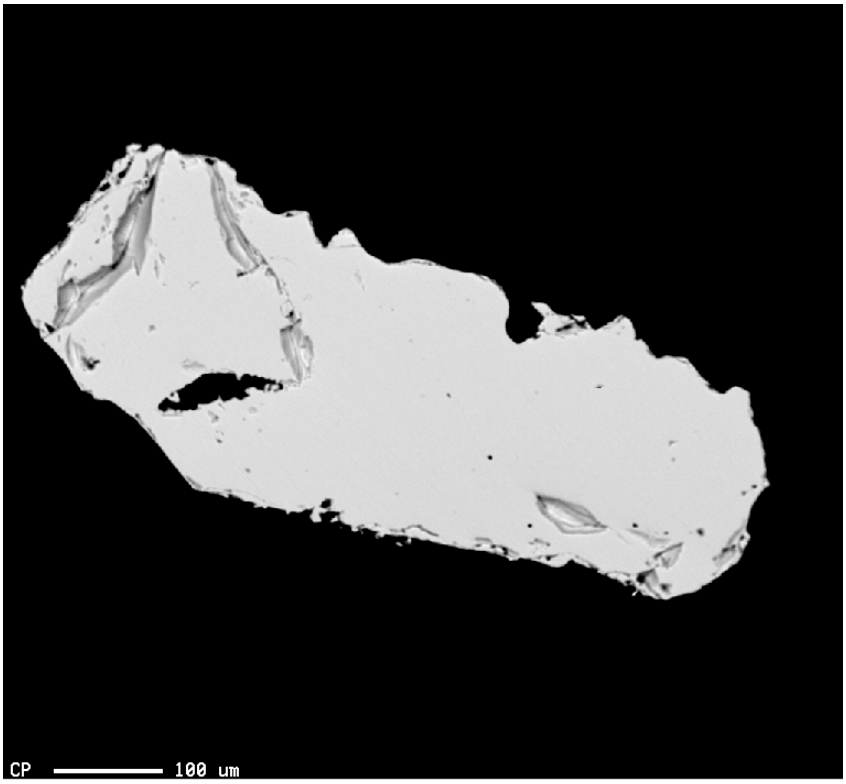

(Figure 8) A backscattered electron image from experiment 8

The run products will be analyzed for indium to determine whether the indium concentration has changed relative to the chalcopyrite and sphalerite starting materials. The gold strip was analyzed for indium, copper, and gold. These data, along with the thermodynamic properties estimated for the ternary, was used to calculate the activity of indium in the system.

Methods of Analysis

In order to analyze the run products in the epoxy mounts using the EPMA, a thin carbon coat (200-300**Å**) was thermally evaporated onto the surface. The mounts were loaded into the sample exchange port, and after approximately 4 minutes when the vacuum is appropriate (2 x 10^{-6} torr), loaded into the instrument. An electron beam with a potential of 20 kV was focused on the sample (~1 um in diameter). The beam interaction volume extends to approximately 1.5 μm into the sulfides (under the operating conditions employed in my analyses).

The indium standards used for these analyses were NSB610 glass which has a concentration of 436 ppm, and indium arsenide (InAs) which contains 60.5% indium. Table 4 lists the other standards used for the analyses. The indium Lα x-ray line was used in the analyses. The primary indium peak (In Lα) is located at an L-value of 120.81 mm on the PETH analytical crystal. There is a second order iron peak (Fe Kα) near potential background positions for indium, and must be accounted for in iron-rich phases (e.g. pyrrhotite, chalcopyrite). To overcome this, an asymmetric background approach was taken to avoid the iron peak overlap: the background positions were measured at 117.31 mm (-3.5mm) and 125.81 mm (+5mm) to avoid the overlap.

Element	Standard
Sulfur	Sphalerite – Synthetic
Iron	Pyrrhotite
Indium	Indium arsenide
Copper	Chalcopyrite
Zinc	Sphalerite – Synthetic

(Table 6) Standards used for the EPMA analyses.

The error due to counting statistics represents the primary uncertainties involved in measurement of concentrations in experimental run products. Uncertainties are calculated using standard x-ray counting statistic techniques. The $1\sigma = \frac{\sqrt{N}}{N} * 100\%$. For example, analysis 50, in the run product analysis of experiment 6 (as seen in Appendix V) had an indium concentration of 4,610 ppm. The relative uncertainty for this analysis was 0.1 % and the 1σ error due to counting statistics was is 4.6. The detection limit of indium in, FeS is 20 ppm, ZnS is 40 ppm, $CuFeS_2$ is 40 ppm, $CuInS_2$ is 40 ppm, In2S3 is 100 ppm, and Au is 15 ppm. Detection limits for the elements are: S 38 ppm, Fe 120ppm, In 20ppm, Cu 110 ppm, Zn 180 ppm.

Backscattered electron images, like that in Figure 8, were obtained to view the homogeneity of the mineral grains. Figure 8 shows a chalcopyrite grain that is very homogenous in texture and composition. This is in contrast to Figure 1 which is very heterogeneous.

Results

The gold sensing method in my experiments which utilized a strip of gold foil in the experimental charge yielded promising results. After 360 hours, the gold, sphalerite, and chalcopyrite were beginning to approach equilibrium. This is observed in Figures 9 and 10 where the concentration of indium in the respective phases begins to asymptotically approach a given value. The concentration of indium in the mineral phases is plotted versus time in Figure 9. Although the values for sphalerite appear to be zero they simply have a very low concentration. Figure 10 shows the indium increase in gold and the leveling off of the concentration around 0.03 wt %.

My experiments yielded an activity of indium in the gold = 0.005182. This activity of indium is equal to the concentration of indium and the activity coefficient is assumed to be 1. The value of 0.005182 is then plugged into equation 16 to obtain the activity of $InCl^{2+}$ in the system for a given pH, molality of Cl-, and fugacity of H_2O and O_2. Again, the activity of $InCl^{2+}$ can be considered equal to the concentration (i.e., the activity coefficient is equal to 1). A series of calculations were performed at differing pH levels to observe the effect of pH on the concentration of indium in the hydrothermal fluid. A positive correlation, as seen in Figure 11,

shows that an increase in acidity results in an increase in indium concentration in the hydrothermal fluid. In fact, the pH has the largest effect on the concentration of indium. The other activities and fugacities in equation 6 are based on values that are characteristic of ore environments. These values can be varied but have little effect when compared to the pH, because the activity of hydrogen ion (also given by 10^{-pH}) is cubed. Limitations arise from the fact that this is only one complex of indium, and therefore these results likely represent minimum aqueous concentrations of In. Since other complexes are unavailable the calculated aqueous concentrations could be low by an order of magnitude or more.

The thermodynamic model developed from the available thermodynamic data was used to calculate the equilibrium constant in equation 15. Equation 15 relates the equilibrium constant to the activities of all of the components.

$$K_{Eq.9} = 10^{2.92} = \frac{a_{FeS}^2 * a_{CuInS_2}}{a_{CuFeS_2} * a_{FeS_2} * a_{In}^{foil},} \qquad \text{Eq. 15}$$

Further, it relates all of the thermodynamic data at 500°C and presents a way to calculate the activity of indium in a hydrothermal ore system given any roquesite component in sphalerite. The model that relates Xroq to thermodynamic parameters in ore-forming systems can inform explorationists regarding the possible exploration guides to finding In ores (e.g., how fO_2, magmatic fractionation, and pH can affect ore formation).

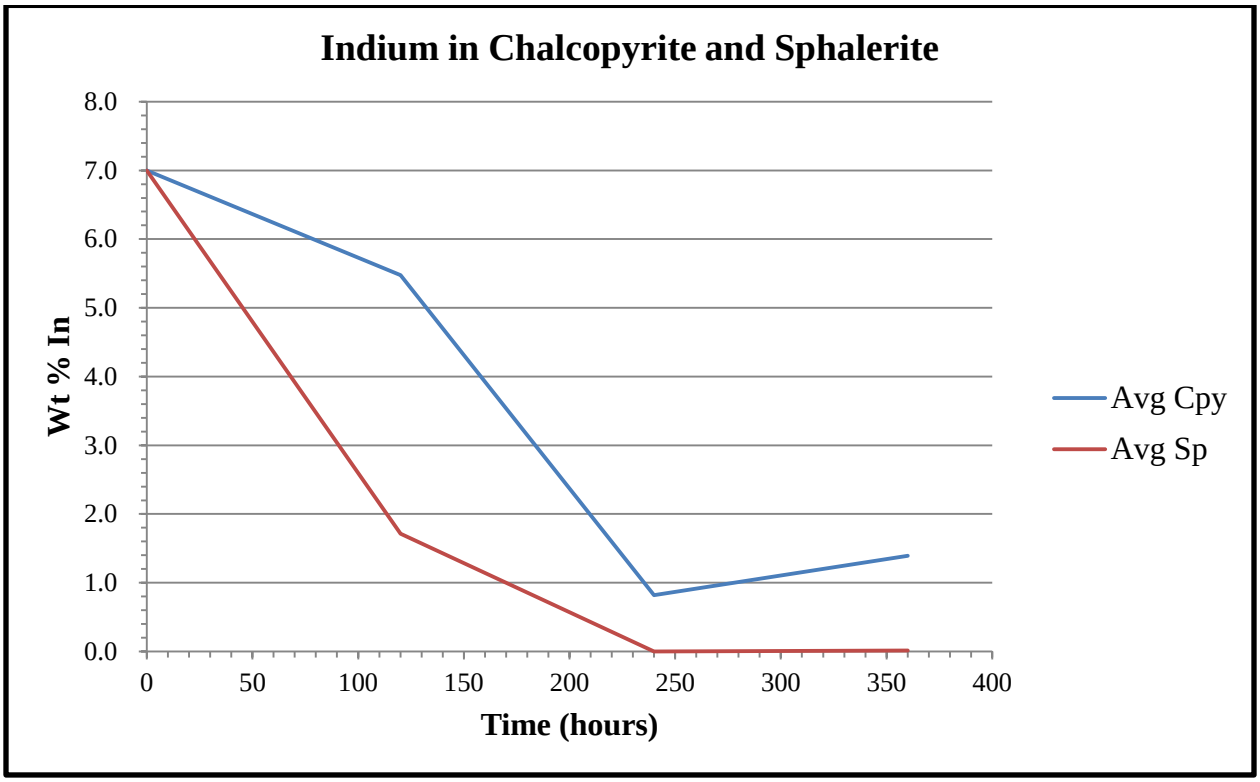

(Figure 9) Graph demonstrating approach to equilibrium in the chalcopyrite and sphalerite.

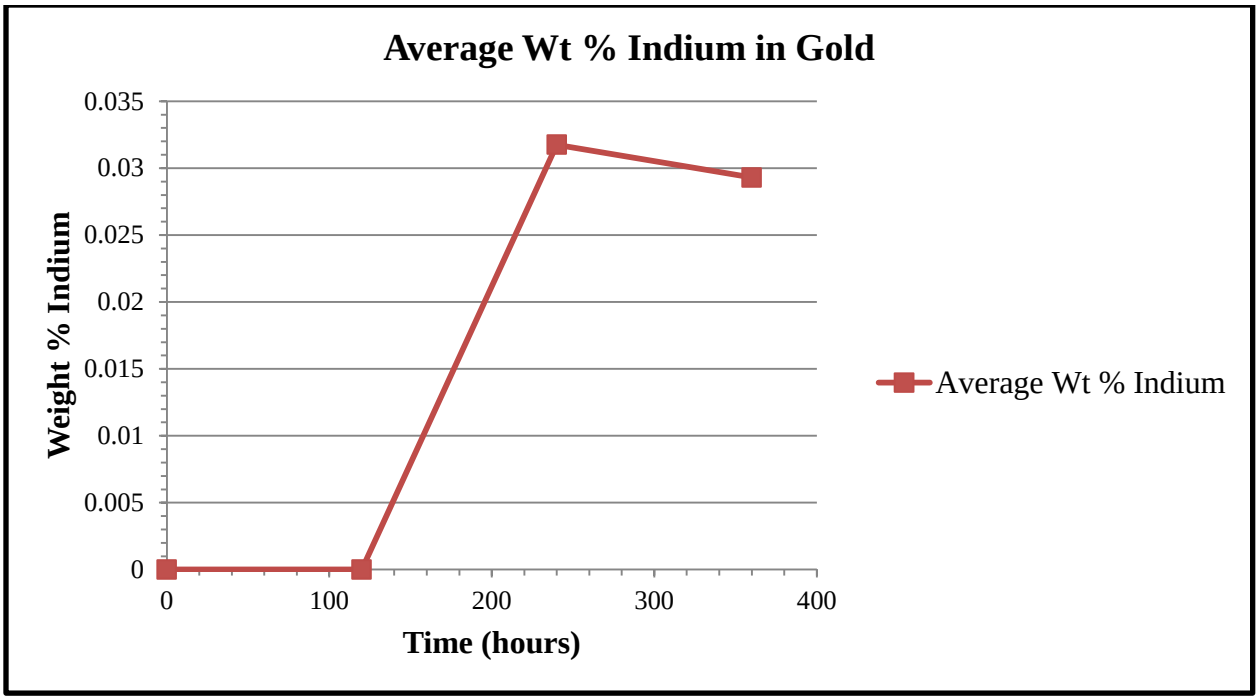

(Figure 10) Graph demonstrating approach to equilibrium in the gold.

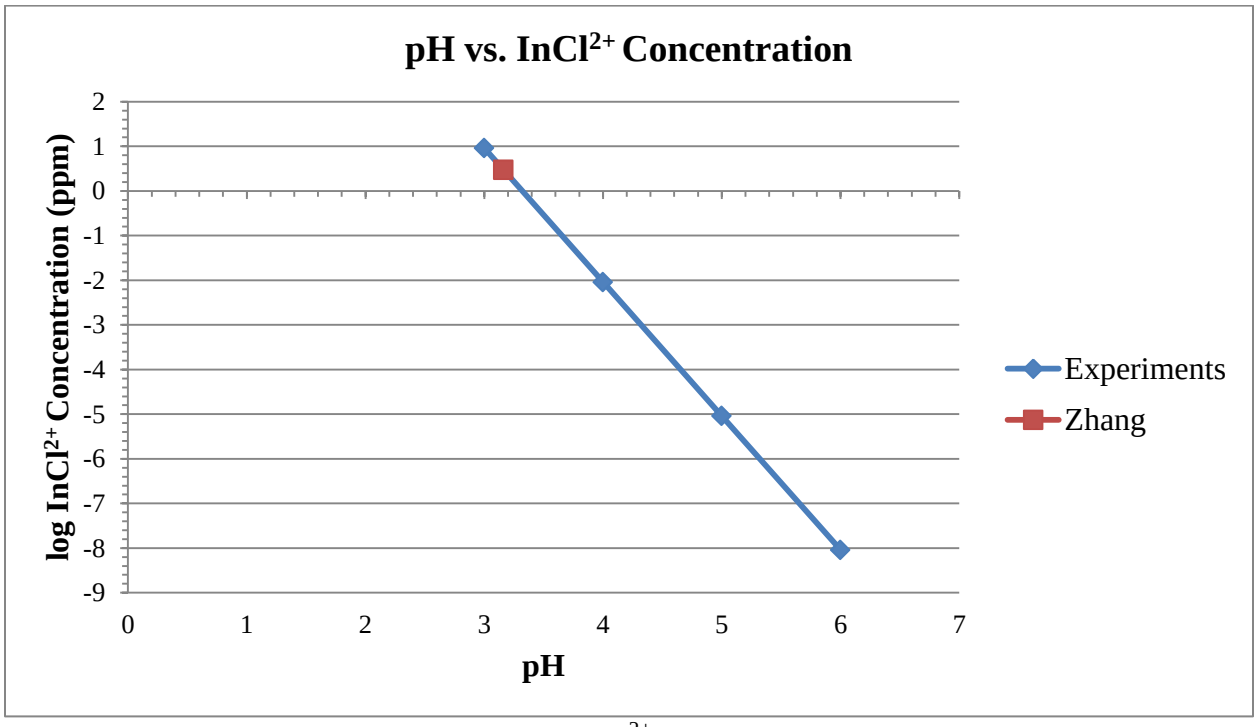

(Figure 11) Graph showing effect of pH on $InCl^{2+}$ concentration. The pH for the average indium concentration in the fluid inclusions from Zhang et al (2007) is also plotted.

Future Work

Future work should involve more experiments with varying indium concentrations and greater time durations to get a more accurate representation of the thermodynamics involved in the system.

Conclusions

I present the groundwork for experiments and thermodynamic modeling for indium-bearing ore systems. The balanced chemical reactions show the functional dependence of how the composition of roquesite depends on aqueous $InCl^{2+}$. That is, for a given aqueous $InCl^{2+}$ concentration, how does aqueous Cl^-, pH, fO_2 change the composition of roquesite? The pH is the determining factor in this system. Papers on the Toyoha mine, cf. Shimizu and Morishita, (2012), suggest that the ore fluid was neutral to acidic.

Sphalerite must be present in the system in order for the roquesite component to be incorporated into the crystallizing sphalerite. Based on a consilience of inductions from my experimental data, I can say that a mole fraction of roquesite equal to 0.03, such as those found at the Toyoha mine, requires a minimum of 9 ppb indium at pressures of hundreds of bars and temperatures up to 500°C, at pH ~3.

Experimentally, the mole fraction of roquesite in sphalerite (0.00011) is in equilibrium with the gold foil that has a mole fraction of 0.000019 (~activity of indium in the system), then a mole fraction of roquesite in sphalerite equal to 0.03, would yield activity of indium in the system = to 0.0052, which is also equal to mole fraction of indium in the gold.
Then, this activity of indium in the system would yield an ore fluid with an $InCl^{2+}$ molality (assuming activity coefficient = 1) on the order of $10^{-11.5}$ to 10^{-3} mol/kg, at a pH of 5.73 (neutral at 500C, 100MPa) and 3, respectively. By using starting materials with a known indium concentration, I was able to monitor the change in indium content of the minerals in the system of interest, as evidenced in Figures 7 and 8.

The Zhang et al. (2007) values of 1.9 to 4.1 ppm indium in the ore fluid are concentrations prior to deposition and compared to my calculations where 99.9 % of the indium has precipitated out. My experiments agree with the hypothesis given a number of assumed geologic standards for fO_2, pH, and molality of Cl^-.

Acknowledgments

I would like to thank Dr. Candela and Dr. Piccoli for all their guidance and support during this process.

Bibliography

Boorman, R.S., and Abbott, D., 1967, Indium in Co-existing Minerals from the Mount Pleasant Tin Deposit: Canadian Mineralogist, v. 9, p. 166-179

Burke, E.A.J., and Kieft, C. (1980) Roquesite and Cu-In-bearing sphalerite from Lfingban, Bergslagen, Sweden. Canadian Mineralogist v. 18, p. 361-363

Chou, K.C., 1995, A General Solution Model for Predicting Ternary Thermodynamic Properties: Calphad, v. 19, No. 3, p. 315-325.

F*A*C*T database (http://www.crct.polymtl.ca/fact/index.php)

Franklin, J.M., Gibson, H.L., Jonasson, I.R., and Galley, A.G., 2005, Volcanogenic Massive Sulfide Deposits, *in* Hedenquist, J.W., Thompson, J.F.H., Goldfarb, R.J., and Richards, J.P., eds., Economic Geology 100th Anniversary Volume: The Economic Geology Publishing Company, p. 523-560

Fryklund, V.C., and Fletcher., J.D., 1956, Geochemistry of Sphalerite from the Star Mine, Coeur d'Alene District, Idaho: Economic Geology, v.51:3, p. 223-247

Galley, A.G., Hannington, M.D., and Jonasson, I.R., 2007, Volcanogenic massive sulphide deposits, *in* Goodfellow, W.D., ed., Mineral Deposits of Canada: A Synthesis of Major Deposit-Types, District Metallogeny, the Evolution of Geological Provinces, and Exploration Methods: Geological Association of Canada, Mineral Deposits Division, Special Publication No. 5, p. 141-161.

Ghosh, D.S., Betancur, R., Chen, T.L., Pruneri, V., and Martorell, J., 2011, Semi-transparent metal electrode of Cu–Ni as a replacement of an ITO in organic photovoltaic cells: Solar Energy Materials and Solar Cells, v. 95:4, p. 1228-1231.

Goldschmidt, V.M., 1937, The principles of distribution of chemical elements in minerals and rocks: Journal of the Chemical Society, p. 655-673

Hou, Z., Khin, Z., Qu, X., Ye Q., Yu, J., Xu, M., Fu, D., and Yin, X, 2001, Origin of the Gacun Volcanic-Hosted Massive Sulfide Deposit in Sichuan, China; Fluid Inclusion and Oxygen Isotope Evidence: Economic Geology, v. 96, p. 1491-1512.

Johan, Z., 1988, Indium and Germanium in the Structure of Sphalerite: an Example of Coupled Substitution with Copper: Mineralogy and Petrology, v. 39, p. 211-229.

Johnson, J.W., Oelkers, E.H., and Helgeson, H.C., 1992, SUPCRT92: A software package for calculating the standard molal thermodynamic properties of minerals, gases, aqueous species, and reactions from 1 to 5000 bar and 0 to 1000°C: Computers & Geosciences, v. 18:7, p. 899-947.

Kieft, K., and Damman, A. H., 1990, Indium-bearing chalcopyrite and sphalerite from the Gfisborn area, West Bergslagen, central Sweden: Mineralogical Magazine, v. 54, p. 109-112.

Kim, Y. H., Sachse, C., Machala, M. L., May, C., Müller-Meskamp, L. and Leo, K., 2011, Highly Conductive PEDOT:PSS Electrode with Optimized Solvent and Thermal Post-Treatment for ITO-Free Organic Solar Cells: Advanced Functional Materials, v. 21, p. 1076–1081.

Liu, Y., Li, Y., and Zeng, H., 2013 ZnO-Based Transparent Conductive Thin Films: Doping, Performance, and Processing; Journal of Nanomaterials, v. 2013, p. 1-9

Liu, H.S., Cui, Y., Ishida, K., and Jin, Z.P., 2002, Thermodynamic Reassessment of the Au-In Binary System: Calphad, v. 27, No 1, p. 27-37.

Liu, H.S., Liu, X.J., Cui, Y., Wang, C.P., Ohnuma, I., Kainuma, R., Jin, Z.P., and Ishida, K., 2002, Thermodynamic Assessment of the Cu-In Binary System: Journal of Phase Equilibria, v. 23, No. 5, p. 409-415.

Metal Prices, Indium Price Charts: http://www.metalprices.com/pubcharts/Public/Indium_Price_Charts.asp (accessed November, 2013).

Migge, H., and Grzanna, J., 1993, Thermochemistry in the system Cu-In-S at 723 K: Journal of Materials Research, v. 9, no. 1, p. 125-131

Murakami, H., and Ishihara, S., 2013, Trace elements of Indium-bearing sphalerite from tin-polymetallic deposits in Bolivia, China and Japan: A femto-second LA-ICPMS study: Ore Geology Reviews, v. 53, p. 223–243

Oen, I. S., Kager, P., and Kieft, C., 1980, Oscillatory Zoning of a Discontinuous solid-solution series: sphalerite-stannite: American Mineralogist, v. 65, p. 1220-1232.

Rudnick, R.L. and Gao, S., 2003, The Composition of the Continental Crust, *in* Holland H.D., and Turekian, K.K., eds., The Crust: Treatise on Geochemistry, v. 3, p. 1-64.

Schwarz-Schampera, U., and Herzig, P.M., 2002, Indium: Geology, Mineralogy, and Economics: Heidelberg, Springer, 257 p.

Shimizu, T., and Morishita, Y., 2012, Petrography, Chemistry, and Near-Infrared Microthermometry of Indium-Bearing Sphalerite from the Toyoha Polymetallic Deposit, Japan: Economic Geology, v. 107, p. 723-735.

Shikazono, N., and Shimizu, M., 1992, Associated Metals in Vein-Type Deposits in Japan: Interpretation Using the HSAB Principle: Canadian Mineralogist, v. 30, p. 137-143.

Toulmin, P., and Barton, P.B., 1963, A Thermodynamic Study of Pyrite and Pyrrhotite: Geochemica et Cosmochimica Acta, v. 28, p. 641-671.

U.S. Geological Survey, 2013, Mineral commodity summaries.

Zhang, Q., Zhu, X., He, Y., and Zhu, Z., 2007, In, Sn, Pb and Zn Contents and Their Relationships in Ore-forming Fluids from Some In-rich and In-poor Deposits in China: Acta Geologica Sinica, v. 81, No. 3, p. 450-462.

Appendix I – Experimental Equipment

Furnace:

The vertical furnace is a Kanthal/Nichrome-wound tube style furnace. The furnace is doubly wound with primary and secondary heating elements being wrapped around a central tube to minimize temperature gradients. High temperature cement is used to make the bulk of the furnace body surrounding the heating elements. The heating elements are connected to a temperature control unit. A thermocouple set within the open tube measures the temperature in the furnace. These readings are relayed back to the temperature control unit.

Thermocouple:

The thermocouple is a piece of equipment used to measure temperature. It consists of 2 dissimilar metals joined on one end that produce a temperature dependent voltage when the temperature changes. The voltage is "read" by the temperature control to indicate what the temperature is at the tip of the thermocouple.

Temperature controller:

The temperature controller is the interface between the furnace and the thermocouple. As the thermocouple indicates the temperature within the tube the controller turns the heating elements on or off depending on if the temperature needs to be increased or decreased.

Appendix II – Composition (weight %) of Sphalerite, Pyrrhotite, Chalcopyrite and Indium-Sulfide in Run Products from Experiments 1, 2, and 4. b.d.l. indicates the element in that analysis is below the detection limit of the EPMA. Detection limits are: S 38 ppm, Fe 120ppm, In 20ppm, Cu 110 ppm, Zn 180 ppm.

Pyrrhotite	**No.**	**S**	**Fe**	**In**	**Cu**	**Zn**	**Total**
Experiment 1	58	39.11	59.45	b.d.l.	1.19	0.01	99.75
	59	39.07	59.44	b.d.l.	1.16	0.00	99.68
	60	39.31	59.67	0.0043	1.19	0.03	100.20
	61	39.07	59.29	0.0473	1.60	0.01	100.01
	62	39.15	59.58	0.0037	1.12	b.d.l.	99.86
	63	39.13	59.92	0.0037	0.82	b.d.l.	99.88
	64	39.22	59.86	0.0521	0.73	b.d.l.	99.86
	65	39.25	59.97	0.0135	0.60	b.d.l.	99.84
	66	38.73	59.58	0.0089	0.95	0.03	99.29
	67	39.38	59.82	0.0245	0.84	b.d.l.	100.07
	68	39.18	59.71	0.0296	0.99	0.02	99.93

Table I.1 Microprobe data for pyrrhotite in experiment 1.

Pyrite	**No.**	**S**	**Fe**	**In**	**Cu**	**Zn**	**Total**
Experiment 1	8	38.79	58.55	0.0043	1.04	b.d.l.	98.39
	69	53.25	47.91	0.0022	0.12	0.08	101.36
	70	53.02	48.05	0.0048	0.05	b.d.l.	101.12
	71	53.46	48.23	0.0074	0.02	0.02	101.74
	72	53.11	47.83	b.d.l.	0.03	0.03	101.00
	73	51.50	47.34	b.d.l.	0.10	0.04	98.98

Table I.2 Microprobe data for pyrite in experiment 1.

Chalcopyrite	No.	S	Fe	In	Cu	Zn	Total
Experiment 1	5	35.25	40.14	b.d.l.	24.73	0.03	100.15
	9	34.60	36.50	b.d.l.	29.06	0.11	100.27
	10	34.52	36.68	0.0072	28.90	0.09	100.19

	11	34.19	36.49	0.0968	28.73	0.06	99.57
	12	34.38	36.34	0.0652	28.75	0.07	99.61
	35	34.18	39.53	b.d.l.	24.75	0.36	98.82
	36	34.37	39.38	b.d.l.	24.81	0.38	98.94
	37	34.56	39.41	0.0217	24.73	0.40	99.12
	38	34.49	39.06	0.5085	24.83	0.44	99.32
	39	34.06	36.34	4.44	24.53	0.59	99.96
	40	34.40	37.91	3.17	24.51	0.01	99.99
	41	34.55	38.84	1.93	24.59	b.d.l.	99.91
	42	34.85	38.67	b.d.l.	24.85	0.13	98.49
	44	35.20	39.68	b.d.l.	25.00	0.08	99.96
	45	35.39	39.45	b.d.l.	25.21	0.15	100.20
	46	34.23	35.82	4.39	24.53	0.77	99.74
	47	34.55	35.81	b.d.l.	28.55	0.08	98.98
	48	34.32	35.87	b.d.l.	28.62	0.07	98.87
	49	34.34	35.90	0.0181	28.57	0.07	98.90
	50	34.50	35.41	0.5715	29.78	0.07	100.32
	51	33.25	30.42	7.5923	29.42	0.11	100.80
	52	34.63	39.62	0.0968	24.05	0.94	99.34
	53	34.55	39.46	0.3816	24.31	0.90	99.59
	54	34.50	38.95	1.1214	24.23	0.86	99.67
	55	33.50	33.62	8.5041	23.34	1.22	100.19
Experiment 2	23	35.66	36.48	b.d.l	25.95	2.70	100.78
	24	35.89	37.10	b.d.l	25.91	2.75	101.64
	24	35.71	36.51	b.d.l	25.90	2.75	100.87
	25	36.00	37.07	b.d.l	25.83	2.75	101.65
	25	35.82	36.48	b.d.l	25.82	2.75	100.87
	26	35.66	36.40	b.d.l	25.85	2.80	100.71
	27	35.81	36.29	0.0056	25.73	2.86	100.69
	28	35.89	36.29	0.0059	25.83	2.89	100.90
Experiment 4	41	35.01	33.54	0.2368	28.98	2.58	100.35
	42	35.25	33.49	0.2252	28.97	2.58	100.50
	43	35.35	33.82	0.2037	28.58	2.56	100.51
	44	34.63	29.75	3.96	28.51	4.42	101.27
	45	34.75	30.83	3.20	29.16	2.99	100.93
	46	35.02	30.81	3.18	29.32	2.99	101.33
	47	51.24	46.10	0.0198	0.75	0.11	98.21

Table I.3 Microprobe data for chalcopyrite in experiments 1, 2, and 4.

Sphalerite	**No.**	**S**	**Fe**	**In**	**Cu**	**Zn**	**Total**
Experiment 1	4	33.07	0.11	0.0055	b.d.l.	67.36	100.55
	7	32.89	0.14	0.0058	b.d.l.	67.03	100.06
	13	32.66	0.13	b.d.l.	b.d.l.	66.95	99.74
	14	33.08	0.11	b.d.l.	b.d.l.	67.13	100.32
	15	32.10	0.17	b.d.l.	b.d.l.	66.43	98.70
	16	33.11	0.14	b.d.l.	0.01	67.03	100.29
	17	33.02	0.16	b.d.l.	b.d.l.	66.52	99.69
	18	32.70	0.17	b.d.l.	b.d.l.	66.57	99.44
	19	32.29	0.18	b.d.l.	b.d.l.	66.44	98.90
	20	32.88	0.17	b.d.l.	0.01	66.90	99.96

	21	32.94	0.21	b.d.l.	b.d.l.	66.68	99.83
	22	33.15	0.21	b.d.l.	b.d.l.	66.73	100.09
	23	32.15	0.23	b.d.l.	b.d.l.	66.55	98.92
	24	32.70	0.23	b.d.l.	b.d.l.	67.18	100.11
	25	33.34	0.21	0.0023	b.d.l.	67.09	100.64
	26	33.22	0.20	b.d.l.	b.d.l.	66.93	100.35
	27	32.99	0.15	b.d.l.	0.01	67.33	100.48
	28	33.04	0.16	b.d.l.	b.d.l.	67.19	100.39
	29	33.12	0.16	0.0102	0.03	66.77	100.10
	30	33.02	0.18	0.0370	0.04	66.25	99.53
	31	33.07	0.27	b.d.l.	0.03	66.51	99.87
	32	33.40	0.26	b.d.l.	0.04	66.59	100.30
	33	33.08	0.34	b.d.l.	0.11	66.83	100.36
	34	33.39	0.24	b.d.l.	0.04	66.95	100.62
Experiment 2	1	33.53	1.99	0.0240	0.25	62.95	98.74
	2	33.56	2.02	0.0278	0.25	63.07	98.93
	3	33.50	2.04	0.0343	0.29	62.95	98.81
	5	30.69	7.97	23.44	14.14	23.46	99.70
	6	33.90	1.44	0.0262	0.26	64.64	100.27
	7	33.47	4.91	4.06	2.34	55.04	99.82
	8	32.94	6.32	8.59	5.38	45.95	99.17
	9	31.37	7.75	19.02	11.54	29.81	99.49
	10	31.25	8.27	19.75	12.31	27.49	99.06
	12	33.91	1.26	0.0264	0.33	63.00	98.53
	16	33.34	4.11	2.06	1.52	57.27	98.29
	17	32.94	5.50	6.52	3.90	49.72	98.59
	18	31.30	7.15	17.45	10.68	32.59	99.16
	21	33.79	7.44	11.02	6.42	40.55	99.22

Table I.4 Microprobe data for sphalerite in experiments 1 and 2.

Indium Sulfide	**No.**	**S**	**Fe**	**In**	**Cu**	**Zn**	**Total**
Experimemt 1	1	27.09	0.24	40.83	23.09	9.89	101.15
	2	26.91	0.06	49.18	20.41	3.64	100.20
	3	28.03	0.07	60.86	7.96	2.76	99.68
	4	26.97	0.07	52.27	17.65	3.21	100.17
	5	28.05	0.07	62.46	6.65	2.60	99.84
	6	28.32	0.07	62.89	6.19	2.53	99.99
	7	28.34	0.08	62.76	6.18	2.59	99.95
	8	28.44	0.05	62.79	6.17	2.55	100.01
	9	28.57	0.09	63.06	6.21	2.53	100.45
	10	28.63	0.08	62.94	6.16	2.60	100.40
	11	28.58	0.06	62.61	6.17	2.55	99.97
	12	28.51	0.05	62.97	6.16	2.46	100.15
	13	28.59	0.05	62.67	6.21	2.53	100.06
	14	28.56	0.06	63.55	6.20	2.52	100.89
	15	28.43	0.05	62.78	6.18	2.53	99.97
	16	28.67	0.05	62.88	6.04	2.51	100.14
	17	28.69	0.04	63.18	6.02	2.52	100.45
	18	28.57	0.02	62.83	6.09	2.51	100.02
	19	28.62	0.07	62.91	6.08	2.52	100.20

	20	28.70	0.05	63.09	6.08	2.55	100.46
	21	26.64	0.48	48.51	25.16	0.82	101.60
	22	28.25	0.35	61.00	9.40	1.55	100.55
	23	28.56	0.34	63.47	6.27	1.88	100.52
	24	28.80	0.31	63.53	6.14	2.08	100.87
	25	28.50	0.29	63.00	6.09	2.30	100.19
	26	28.56	0.21	64.77	7.26	0.00	100.80
	27	28.55	0.16	64.51	7.33	0.00	100.54
	28	28.54	0.11	64.72	7.34	0.00	100.72
	29	28.58	0.10	64.69	7.37	0.01	100.74
	30	28.64	0.06	64.91	7.41	0.00	101.03
Experiment 2	29	30.57	8.06	27.57	15.84	18.58	100.62
	30	29.77	7.86	25.29	14.89	20.92	98.74
	31	29.68	8.40	26.67	15.67	18.82	99.24
	32	28.25	4.27	38.01	21.13	8.70	100.36
	36	29.55	6.84	31.69	18.53	14.11	100.72
	37	29.11	5.77	35.01	20.18	11.35	101.42
	40	29.59	6.49	32.19	18.79	14.25	101.32
Experiment 4	48	27.29	3.39	42.05	25.15	3.25	101.13
	50	26.09	4.51	39.52	22.12	7.25	99.48

Table I.5 Microprobe data for indium sulfide phases in experiments 1, 2, and 4.

Appendix III – Uncertainty due to counting statistics for the EPMA.

Analysis #	**In**	**Fe**	**S**	**Cu**	**Zn**	**Analysis #**	**In**	**Fe**	**S**	**Cu**	**Zn**
1	9.71	0.96	0.13	5.03	0.15	**31**	0.14	0.44	0.05	0.31	0.29
2	0.14	0.95	8.41	4.96	0.15	**32**	0.14	0.65	0.04	0.26	0.45
3	0.14	0.95	6.87	4.43	0.15	**33**	0.14	1.20	0.04	0.24	1.00
4	0.19	0.58	0.08	0.44	0.32	**34**	0.14	1.06	0.04	0.24	0.97
5	0.14	0.44	0.05	0.31	0.25	**35**	0.14	1.04	0.04	0.24	0.98
6	0.13	1.16	8.13	4.88	0.15	**36**	0.14	0.50	0.05	0.28	0.34
7	0.13	0.57	0.15	0.89	0.16	**37**	0.14	0.55	0.05	0.27	0.38
8	0.13	0.50	0.09	0.54	0.18	**38**	0.14	0.69	0.04	0.25	0.48
9	0.14	0.45	0.06	0.35	0.22	**39**	0.14	0.55	0.05	0.27	0.37
10	0.14	0.44	0.06	0.34	0.23	**40**	0.14	0.51	0.05	0.28	0.34
11	0.19	0.62	0.08	0.45	0.30	**41**	0.13	0.21	1.02	0.23	0.97
12	0.14	1.29	8.92	3.96	0.15	**42**	0.13	0.21	1.08	0.23	0.97
13	0.14	1.09	1.42	3.39	0.15	**43**	0.13	0.21	1.17	0.23	0.98
14	0.14	0.62	0.16	0.99	0.16	**44**	0.13	0.23	0.15	0.23	0.68
15	0.14	1.27	12.34	3.89	0.15	**45**	0.13	0.22	0.17	0.22	0.88
16	0.14	0.63	0.23	1.21	0.16	**46**	0.13	0.22	0.17	0.22	0.88
17	0.14	0.54	0.12	0.66	0.17	**47**	0.10	0.19	10.93	1.95	14.04
18	0.14	0.48	0.07	0.37	0.21	**48**	0.15	0.75	0.04	0.24	0.85
19	0.14	0.54	0.13	0.79	0.17	**49**	0.14	0.75	0.04	0.24	0.81
20	0.14	0.70	0.59	2.60	0.16	**50**	0.15	0.64	0.04	0.25	0.50
21	0.13	0.47	0.09	0.49	0.19	**51**	0.11	0.19	0.32	1.68	4.61
22	0.16	0.55	0.08	0.50	0.30	**52**	0.14	100.00	39.20	100.00	0.15
23	0.13	0.20	100.00	0.24	0.93	**53**	0.14	560.56	100.00	100.00	0.15
24	0.13	0.20	100.00	0.24	0.91	**54**	0.14	100.00	100.00	100.00	0.15
25	0.13	0.20	226.32	0.24	0.91	**55**	0.14	0.84	100.00	100.00	0.15
26	0.13	0.20	100.00	0.24	0.91	**56**	0.14	0.83	208.85	100.00	0.15
27	0.13	0.20	36.43	0.24	0.90	**57**	0.14	0.82	100.00	103.56	0.15
28	0.13	0.20	34.82	0.24	0.89	**58**	0.12	0.16	100.00	23.07	44.16

29	0.14	0.45	0.05	0.30	0.29	**59**	0.12	0.16	116.93	26.12	282.65
30	0.14	0.46	0.05	0.31	0.27	**60**	0.12	0.16	100.00	24.31	100.00
						61	0.12	0.16	100.00	38.06	100.00

Table I.6 Uncertainties calculated in the microprobe software. This is all for experiment 1 analyses.

Appendix IV. Additional backscattered images to show textures and phases.

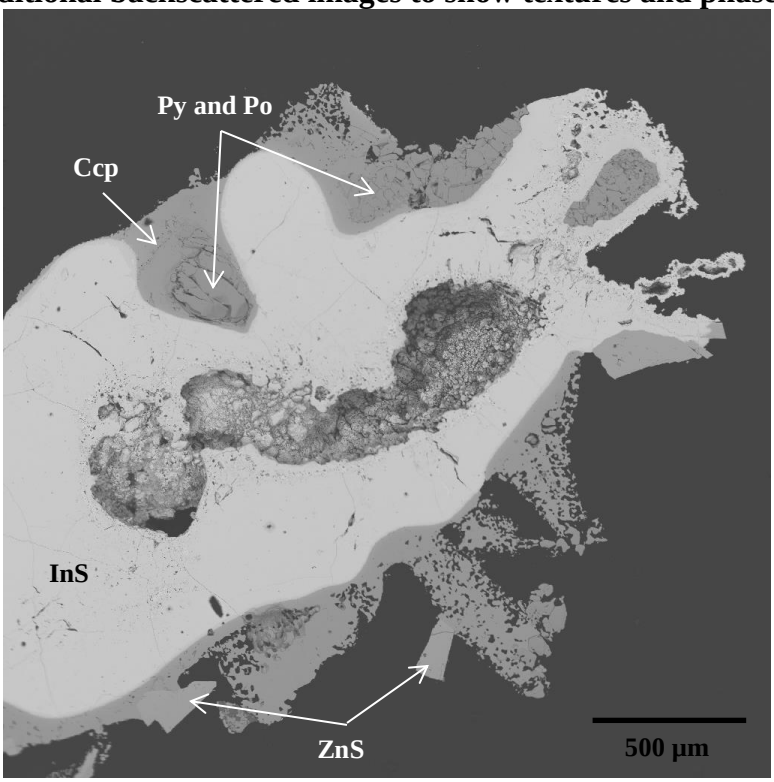

Figure I.1 Experiment 1 - Grain 2. Indium sulfide phase, copper rich rim. Chalcopyrite, pyrite, and pyrrhotite present.

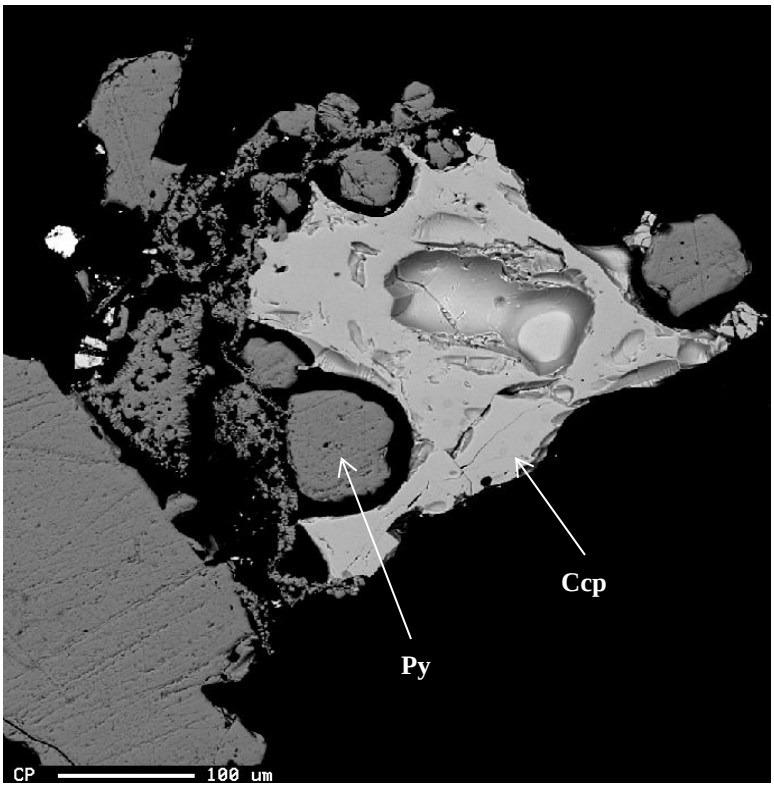

Figure I.2 Experiment 2. Large chalcopyrite grain with pyrite grains surrounding it.

Appendix V – Run analyses from Geology 394

The detection limit of indium in, FeS is 20 ppm, ZnS is 40 ppm, $CuFeS_2$ is 40 ppm, $CuInS_2$ is 40 ppm, In2S3 is 100 ppm, and Au is 15 ppm. Detection limits for the elements are: S 38 ppm, Fe 120ppm, In 20ppm, Cu 110 ppm, Zn 180 ppm. b.d.l. stands for below detection limit.

Gold run product analyses (in weight percent) and initial gold followed by uncertainties due to counting statistics.

No.	In	Fe	S	Cu	Zn	Au	Total	Run #
1	b.d.l.	b.d.l.	b.d.l.	0.012	b.d.l.	97.63	97.65	Initial Au
2	b.d.l.	b.d.l.	b.d.l.	b.d.l.	b.d.l.	99.13	99.13	Initial Au
3	b.d.l.	b.d.l.	b.d.l.	0.015	b.d.l.	98.06	98.08	Initial Au
4	b.d.l.	b.d.l.	b.d.l.	b.d.l.	b.d.l.	98.42	98.44	Initial Au
5	b.d.l.	b.d.l.	b.d.l.	b.d.l.	b.d.l.	100.08	100.08	Initial Au
6	b.d.l.	b.d.l.	b.d.l.	b.d.l.	b.d.l.	100.16	100.17	Initial Au
7	b.d.l.	b.d.l.	b.d.l.	b.d.l.	b.d.l.	98.59	98.59	Initial Au
8	b.d.l.	b.d.l.	b.d.l.	b.d.l.	b.d.l.	98.58	98.59	Initial Au
9	b.d.l.	b.d.l.	b.d.l.	b.d.l.	b.d.l.	96.72	96.72	Initial Au
10	b.d.l.	b.d.l.	b.d.l.	b.d.l.	b.d.l.	97.23	97.25	Initial Au
11	b.d.l.	b.d.l.	b.d.l.	b.d.l.	b.d.l.	97.23	97.23	Initial Au
12	b.d.l.	b.d.l.	b.d.l.	b.d.l.	b.d.l.	99.59	99.59	Initial Au
13	b.d.l.	b.d.l.	0.024	0.080	b.d.l.	99.33	99.44	6

14	b.d.l.	b.d.l.	b.d.l.	b.d.l.	b.d.l.	99.31	99.32	6
15	b.d.l.	b.d.l.	0.012	b.d.l.	b.d.l.	99.06	99.07	6
16	b.d.l.	b.d.l.	b.d.l.	0.014	b.d.l.	98.83	98.86	6
17	b.d.l.	b.d.l.	0.006	b.d.l.	0.017	98.53	98.56	6
18	b.d.l.	b.d.l.	0.009	0.021	b.d.l.	99.02	99.05	6
19	b.d.l.	b.d.l.	0.017	0.106	b.d.l.	99.82	99.94	6
20	b.d.l.	b.d.l.	b.d.l.	0.030	b.d.l.	98.71	98.74	6
21	b.d.l.	b.d.l.	0.005	0.027	b.d.l.	98.38	98.42	6
22	b.d.l.	b.d.l.	0.005	0.000	b.d.l.	98.71	98.72	6
23	b.d.l.	b.d.l.	b.d.l.	0.011	b.d.l.	98.75	98.76	6
24	b.d.l.	b.d.l.	b.d.l.	0.056	b.d.l.	97.54	97.60	6
25	b.d.l.	b.d.l.	b.d.l.	0.074	b.d.l.	94.99	95.08	7
26	b.d.l.	b.d.l.	0.001	0.036	b.d.l.	96.45	96.49	7
27	b.d.l.	b.d.l.	0.005	0.011	b.d.l.	96.06	96.08	7
28	b.d.l.	b.d.l.	0.015	0.020	b.d.l.	95.86	95.90	7
29	b.d.l.	b.d.l.	0.002	b.d.l.	b.d.l.	94.46	94.47	7
30	b.d.l.	b.d.l.	0.002	0.054	0.034	96.05	96.14	7
31	b.d.l.	b.d.l.	0.013	0.017	0.025	84.02	84.08	7
32	b.d.l.	b.d.l.	0.007	0.013	b.d.l.	83.60	83.62	7
33	b.d.l.	b.d.l.	0.003	0.014	b.d.l.	82.75	82.77	7
34	b.d.l.	b.d.l.	0.023	b.d.l.	b.d.l.	82.51	82.54	7
35	b.d.l.	b.d.l.	b.d.l.	b.d.l.	0.035	82.98	83.03	7
36	b.d.l.	b.d.l.	0.003	0.069	b.d.l.	82.93	83.01	7
No.	**In**	**S**	**Au**	**Fe**	**Cu**	**Zn**	**Total**	**Run #**
7	b.d.l.	b.d.l.	100.405	b.d.l.	0.156	b.d.l.	100.57	8
8	b.d.l.	0.058	99.838	0.026	0.081	0.076	100.08	8
9	0.0549	0.233	99.275	0.040	0.195	b.d.l.	99.81	8
10	b.d.l.	0.056	101.482	b.d.l.	0.165	0.055	101.77	9
11	b.d.l.	0.088	102.768	b.d.l.	0.184	0.049	103.10	9
12	b.d.l.	0.054	99.371	0.016	0.068	0.104	99.61	10
13	b.d.l.	0.119	97.273	0.083	0.201	0.047	97.72	10
14	0.0293	0.099	100.101	0.025	0.123	0.045	100.42	11
15	b.d.l.	0.130	97.101	0.055	0.169	0.106	97.56	11
16	b.d.l.	0.156	94.122	b.d.l.	0.144	b.d.l.	94.42	11
17	b.d.l.	0.048	102.898	b.d.l.	0.071	0.092	103.11	11
18	0.0016	0.039	89.394	0.075	0.086	0.063	89.66	10
19	0.0982	0.792	93.014	0.799	0.653	b.d.l.	95.36	10
20	0.0086	0.493	98.135	0.393	0.393	b.d.l.	99.42	9
21	b.d.l.	0.044	97.091	b.d.l.	0.163	b.d.l.	97.30	9
22	b.d.l.	0.223	99.441	b.d.l.	0.215	b.d.l.	99.88	8
23	b.d.l.	0.096	101.083	b.d.l.	0.167	0.025	101.38	8
24	0.0552	0.219	98.501	0.134	0.219	0.048	99.18	8
25	b.d.l.	0.134	98.974	0.051	0.123	b.d.l.	99.28	8

26	b.d.l.	0.110	99.741	0.054	0.198	b.d.l.	100.10	8
27	b.d.l.	0.088	101.128	b.d.l.	0.064	0.032	101.31	8
28	b.d.l.	0.042	102.231	b.d.l.	0.122	b.d.l.	102.39	8
Relative Uncertainties (%)								
No.	**In**	**Fe**	**S**	**Cu**	**Zn**	**Au**	**Total**	**Run #**
1	100.00	623.85	100.00	73.34	89.04	0.14	986.37	Initial Au
2	100.00	7143.33	100.00	320.39	100.00	0.14	7763.86	Initial Au
3	100.00	100.00	100.00	58.54	100.00	0.14	458.68	Initial Au
4	100.00	100.00	100.00	118.61	116.74	0.14	535.49	Initial Au
5	100.00	100.00	100.00	100.00	100.00	0.14	500.14	Initial Au
6	100.00	100.00	100.00	326.92	152.29	0.14	779.35	Initial Au
7	100.00	100.00	100.00	100.00	100.00	0.14	500.14	Initial Au
8	100.00	100.00	100.00	100.00	118.96	0.14	519.10	Initial Au
9	100.00	100.00	100.00	100.00	100.00	0.14	500.14	Initial Au
10	100.00	108.97	100.00	195.17	10239.2	0.14	10743.5	Initial Au
11	100.00	100.00	100.00	100.00	100.00	0.14	500.14	Initial Au
12	100.00	100.00	100.00	100.00	100.00	0.14	500.14	Initial Au
13	100.00	100.00	17.83	11.20	184.41	0.14	413.58	6
14	100.00	111.96	1189.95	346.34	100.00	0.14	1848.39	6
15	100.00	100.00	35.68	141.03	100.00	0.14	476.85	6
16	100.00	107.40	100.00	62.32	141.55	0.14	511.41	6
17	100.00	100.00	67.52	123.69	82.72	0.14	474.07	6
18	100.00	100.00	45.50	41.23	100.00	0.14	386.87	6
19	100.00	100.00	25.55	8.46	100.00	0.14	334.15	6
20	100.00	100.00	100.00	28.84	100.00	0.14	428.98	6
21	100.00	100.00	80.11	32.45	819.03	0.14	1131.73	6
22	100.00	409.26	83.61	100.00	100.00	0.14	793.01	6
23	100.00	114.92	100.00	75.05	100.00	0.14	490.11	6
24	100.00	209.19	100.00	15.66	100.00	0.14	524.99	6
25	100.00	100.00	100.00	11.77	125.12	0.14	437.03	7
26	100.00	100.00	295.62	24.03	100.00	0.14	619.79	7
27	100.00	301.36	94.44	78.34	100.00	0.14	674.28	7
28	100.00	100.00	28.08	42.49	100.00	0.14	370.71	7
29	100.00	100.00	218.46	253.39	182.85	0.14	854.84	7
30	100.00	100.00	181.11	16.06	39.77	0.14	437.08	7
31	100.00	250.45	34.30	49.99	55.06	0.15	489.95	7
32	100.00	100.00	59.54	67.07	100.00	0.16	426.77	7
33	100.00	100.00	125.49	62.01	100.00	0.16	487.66	7
34	100.00	100.00	19.06	100.00	100.00	0.16	419.22	7
35	100.00	183.56	100.00	94.91	39.11	0.16	517.74	7
36	100.00	100.00	145.38	12.62	102.75	0.16	460.91	7
No.	**In**	**S**	**Au**	**Fe**	**Cu**	**Zn**	**Total**	**Run #**
7	100.00	80.92	1.01	1089.78	31.71	100.00	1303.42	8

8	100.00	14.01	1.00	110.10	60.97	77.60	263.68	8
9	2.77	4.33	1.02	74.51	26.03	370.33	476.22	8
10	100.00	14.97	1.00	301.52	28.87	107.43	453.79	9
11	100.00	10.17	0.99	363.17	26.69	124.75	525.77	9
12	100.00	15.33	1.01	183.01	72.48	57.43	329.26	10
13	100.00	8.01	1.04	35.58	24.37	130.70	199.70	10
14	4.95	9.05	1.02	114.52	41.16	139.20	304.95	11
15	100.00	7.45	1.04	52.45	29.50	57.96	148.40	11
16	100.00	6.37	1.06	100.00	34.69	100.00	242.12	11
17	100.00	17.53	0.99	100.00	68.55	65.59	252.66	11
18	101.55	23.29	1.09	38.36	59.34	98.20	220.28	10
19	1.55	1.74	1.07	4.31	8.22	100.00	115.34	10
20	18.54	2.51	1.03	8.23	13.14	100.00	124.91	9
21	100.00	20.05	1.04	100.00	29.56	100.00	250.65	9
22	100.00	4.74	1.02	100.00	23.69	100.00	229.45	8
23	100.00	9.22	1.02	461.87	29.65	244.47	746.23	8
24	2.85	4.70	1.03	21.89	23.39	129.40	180.41	8
25	100.00	6.95	1.01	55.85	40.97	100.00	204.78	8
26	100.00	8.09	1.01	50.16	24.87	100.00	184.13	8
27	100.00	9.82	0.99	100.00	77.93	186.20	374.94	8
28	100.00	19.98	0.99	100.00	38.92	100.00	259.89	8

Run product analyses (in weight percent) and starting sulfides followed by uncertainties due to counting statistics from experiments 6 and 7.

No.	**In**	**Fe**	**S**	**Cu**	**Zn**	**Au**	**Total**	**Run #**	**Phase**
37	0.053	0.405	14.859	0.073	5.043	0.00	20.43	6	ZnS
38	b.d.l.	1.313	31.619	0.162	68.502	0.14	101.73	6	ZnS
39	b.d.l.	1.303	31.135	0.181	68.594	0.07	101.28	6	ZnS
40	b.d.l.	1.290	32.020	0.145	68.805	0.20	102.46	6	ZnS
41	b.d.l.	1.311	27.039	0.037	67.720	0.12	96.23	6	ZnS
42	b.d.l.	1.368	32.074	0.027	68.331	0.09	101.89	6	ZnS
43	0.475	3.820	29.796	0.334	61.163	0.14	95.73	6	ZnS
44	0.015	1.920	31.313	0.154	67.065	0.12	100.59	6	ZnS
45	b.d.l.	1.327	32.329	0.161	68.600	0.13	102.55	6	ZnS
46	b.d.l.	1.343	32.227	0.164	68.596	0.17	102.50	6	ZnS
47	b.d.l.	1.432	31.918	0.059	68.637	0.21	102.25	6	ZnS
48	0.008	1.382	27.073	0.060	65.028	b.d.l.	93.55	6	ZnS
49	b.d.l.	1.437	32.161	0.068	68.246	0.20	102.11	6	ZnS
50	4.614	32.459	33.107	23.036	3.986	b.d.l.	97.20	6	CuFeS2
51	5.298	31.744	31.896	22.919	3.846	b.d.l.	95.70	6	CuFeS2
52	5.751	31.902	32.694	23.262	3.558	b.d.l.	97.17	6	CuFeS2
53	6.119	31.861	33.036	23.362	3.225	b.d.l.	97.60	6	CuFeS2
54	6.344	31.862	33.120	23.702	2.878	b.d.l.	97.90	6	CuFeS2

55	6.942	31.565	33.004	23.684	2.460	b.d.l.	97.66	6	CuFeS2
56	13.935	26.292	31.924	22.743	3.113	b.d.l.	98.01	6	CuFeS2
57	33.943	10.607	28.127	20.984	4.989	b.d.l.	98.65	6	CuFeS2
58	46.329	0.512	26.169	25.307	0.245	b.d.l.	98.56	6	InS
59	46.949	0.123	25.973	25.368	0.072	b.d.l.	98.49	6	InS
60	46.377	0.057	25.720	25.341	0.051	b.d.l.	97.55	6	InS
61	47.012	0.051	26.025	25.556	0.086	b.d.l.	98.73	6	InS
62	46.524	0.090	25.828	24.944	0.224	b.d.l.	97.61	6	InS
63	43.378	0.651	24.393	24.336	0.840	b.d.l.	93.60	6	InS
64	0.126	1.384	30.766	0.130	64.284	0.10	96.79	7	ZnS
65	0.013	1.473	33.026	0.088	67.135	0.14	101.88	7	ZnS
66	0.011	1.500	33.023	0.095	67.156	0.15	101.93	7	ZnS
67	0.058	1.503	33.300	0.131	65.996	0.10	101.09	7	ZnS
68	1.493	3.413	34.193	0.829	61.207	0.18	101.31	7	ZnS
69	5.088	10.882	33.453	3.133	48.241	0.02	100.82	7	ZnS
70	4.847	10.646	32.313	3.036	48.564	b.d.l.	99.41	7	ZnS
71	5.198	10.090	33.032	3.179	49.609	0.09	101.20	7	ZnS
72	5.070	9.642	33.340	3.109	50.666	0.12	101.95	7	ZnS
73	4.870	10.614	32.452	3.049	47.291	0.14	98.41	7	ZnS
74	4.811	11.366	31.241	3.090	48.298	0.10	98.91	7	ZnS
75	5.032	11.073	32.945	3.200	48.668	0.16	101.08	7	ZnS
76	5.991	8.699	32.285	3.646	49.858	0.17	100.65	7	ZnS
77	2.015	1.746	34.543	1.034	61.248	0.23	100.81	7	ZnS
78	3.287	35.264	33.931	23.400	2.404	b.d.l.	98.29	7	CuFeS2
79	3.461	35.455	33.343	23.572	2.136	b.d.l.	97.97	7	CuFeS2
80	3.569	35.537	33.432	23.718	1.946	0.02	98.22	7	CuFeS2
81	3.683	35.403	33.475	23.974	1.930	b.d.l.	98.47	7	CuFeS2
82	4.337	35.050	33.257	24.020	1.864	b.d.l.	98.53	7	CuFeS2
83	5.213	34.408	33.536	24.031	1.868	b.d.l.	99.05	7	CuFeS2
84	5.958	33.839	33.067	23.840	2.036	b.d.l.	98.74	7	CuFeS2
85	6.677	33.233	33.268	23.824	2.133	b.d.l.	99.13	7	CuFeS2
86	8.767	31.658	33.423	23.285	2.495	b.d.l.	99.63	7	CuFeS2
87	31.747	11.878	29.250	19.932	8.675	0.03	101.51	7	CuFeS2
88	43.283	2.825	26.005	24.300	1.658	b.d.l.	98.07	7	InS
89	47.203	0.488	25.956	25.911	0.294	b.d.l.	99.85	7	InS
90	44.283	1.595	25.531	24.943	1.379	b.d.l.	97.73	7	InS
91	29.372	9.958	28.531	18.390	11.642	b.d.l.	97.89	7	InS
92	b.d.l	1.193	32.191	0.150	66.327	b.d.l.	99.86	Initial	ZnS
93	b.d.l	1.234	33.649	0.212	66.395	b.d.l.	101.49	Initial	ZnS
94	b.d.l	1.245	33.866	0.141	66.707	b.d.l.	101.96	Initial	ZnS
95	0.005	1.183	34.089	0.136	66.794	b.d.l.	102.21	Initial	ZnS
96	b.d.l.	1.242	30.899	0.050	65.913	b.d.l.	98.10	Initial	ZnS
97	b.d.l.	1.245	33.039	0.053	66.742	b.d.l.	101.08	Initial	ZnS

98	b.d.l.	1.184	33.200	0.044	66.938	b.d.l.	101.37	Initial	ZnS
99	b.d.l.	1.101	33.311	0.047	67.122	b.d.l.	101.58	Initial	ZnS
100	b.d.l.	1.085	33.785	0.053	67.139	b.d.l.	102.06	Initial	ZnS
101	0.005	0.997	33.933	0.068	67.342	b.d.l.	102.35	Initial	ZnS
102	0.021	24.029	27.836	38.174	0.334	b.d.l.	90.39	Initial	CuFeS2
103	0.017	27.392	31.939	37.548	0.395	b.d.l.	97.29	Initial	CuFeS2
104	0.025	27.896	32.501	36.910	0.357	b.d.l.	97.69	Initial	CuFeS2
105	0.020	28.874	32.830	35.478	0.245	b.d.l.	97.45	Initial	CuFeS2
106	0.019	28.171	32.705	36.667	0.323	b.d.l.	97.88	Initial	CuFeS2
107	0.021	28.595	32.733	35.715	0.309	b.d.l.	97.37	Initial	CuFeS2
108	0.022	29.625	33.240	34.355	0.228	b.d.l.	97.47	Initial	CuFeS2
109	0.023	29.132	32.526	34.466	0.230	b.d.l.	96.38	Initial	CuFeS2
110	0.015	29.328	32.311	34.957	0.148	b.d.l.	96.76	Initial	CuFeS2
111	0.013	29.388	32.709	35.089	0.127	b.d.l.	97.33	Initial	CuFeS2
112	0.024	28.739	32.733	36.026	0.328	b.d.l.	97.85	Initial	CuFeS2
113	0.014	30.399	33.855	35.120	0.115	b.d.l.	99.50	Initial	CuFeS2
114	0.014	30.400	33.641	35.325	0.141	b.d.l.	99.52	Initial	CuFeS2
115	0.013	30.324	33.665	35.134	0.130	b.d.l.	99.27	Initial	CuFeS2
116	0.008	30.260	32.617	35.138	0.120	b.d.l.	98.14	Initial	CuFeS2
117	b.d.l.	25.337	17.281	30.420	0.115	b.d.l.	73.15	Initial	CuFeS2
149	0.004	30.348	33.662	34.781	0.139	b.d.l.	98.94	Initial	CuFeS2
150	0.006	30.328	33.645	34.838	0.122	b.d.l.	98.94	Initial	CuFeS2
151	0.008	30.280	33.387	35.018	0.124	b.d.l.	98.82	Initial	CuFeS2
152	0.022	28.651	32.515	37.250	0.363	b.d.l.	98.80	Initial	CuFeS2
153	0.015	28.095	31.497	38.053	0.386	b.d.l.	98.05	Initial	CuFeS2
154	0.024	28.134	32.551	38.456	0.353	b.d.l.	99.52	Initial	CuFeS2
Relative Uncertainties (%)									
No.	**In**	**Fe**	**S**	**Cu**	**Zn**	**Au**	**Total**	**Run**	**Phase**
37	2.42	1.32	0.13	6.41	0.41	100.00	110.69	6	ZnS
38	100.00	0.69	0.10	4.83	0.10	32.26	137.98	6	ZnS
39	385.08	0.70	0.10	4.34	0.10	63.62	453.94	6	ZnS
40	100.00	0.70	0.10	5.27	0.10	21.91	128.08	6	ZnS
41	100.00	0.67	0.11	18.83	0.10	35.34	155.05	6	ZnS
42	100.00	0.66	0.10	26.38	0.10	51.98	179.22	6	ZnS
43	0.41	0.34	0.10	2.50	0.11	30.28	33.74	6	ZnS
44	10.11	0.52	0.10	5.05	0.11	36.27	52.16	6	ZnS
45	100.00	0.68	0.10	4.80	0.10	33.74	139.42	6	ZnS
46	100.00	0.68	0.10	4.77	0.10	26.83	132.48	6	ZnS
47	100.00	0.65	0.10	12.40	0.10	21.07	134.32	6	ZnS
48	16.74	0.65	0.11	11.71	0.11	100.00	129.32	6	ZnS
49	1778.57	0.63	0.10	10.62	0.10	21.88	1811.9	6	ZnS
50	0.09	0.11	0.09	0.17	0.51	100.00	100.97	6	CuFeS2
51	0.09	0.11	0.09	0.17	0.52	100.00	100.98	6	CuFeS2

52	0.08	0.11	0.09	0.17	0.56	100.00	101.01	6	CuFeS2
53	0.08	0.11	0.09	0.17	0.59	100.00	101.04	6	CuFeS2
54	0.08	0.11	0.09	0.17	0.64	100.00	101.09	6	CuFeS2
55	0.08	0.11	0.09	0.17	0.72	100.00	101.17	6	CuFeS2
56	0.05	0.12	0.09	0.17	0.61	100.00	101.04	6	CuFeS2
57	0.03	0.20	0.10	0.18	0.45	100.00	100.96	6	CuFeS2
58	0.03	1.63	0.10	0.16	5.37	100.00	107.29	6	InS
59	0.03	6.04	0.10	0.16	18.12	100.00	124.45	6	InS
60	0.03	12.82	0.10	0.16	25.40	100.00	138.51	6	InS
61	0.03	14.49	0.10	0.16	15.01	100.00	129.79	6	InS
62	0.03	8.49	0.10	0.16	5.90	100.00	114.68	6	InS
63	0.03	1.29	0.11	0.17	1.76	100.00	103.36	6	InS
64	1.30	0.64	0.10	5.74	0.11	44.41	52.30	7	ZnS
65	11.63	0.62	0.10	8.56	0.10	31.30	52.31	7	ZnS
66	13.61	0.63	0.10	7.87	0.10	30.07	52.38	7	ZnS
67	2.73	0.63	0.10	5.72	0.11	42.85	52.14	7	ZnS
68	0.19	0.37	0.10	1.23	0.11	24.23	26.23	7	ZnS
69	0.09	0.19	0.10	0.52	0.12	182.16	183.18	7	ZnS
70	0.09	0.19	0.10	0.53	0.12	100.00	101.03	7	ZnS
71	0.09	0.20	0.10	0.51	0.12	47.55	48.57	7	ZnS
72	0.09	0.20	0.10	0.52	0.12	34.87	35.90	7	ZnS
73	0.09	0.19	0.10	0.52	0.13	31.43	32.46	7	ZnS
74	0.09	0.18	0.10	0.52	0.12	41.61	42.62	7	ZnS
75	0.09	0.19	0.10	0.50	0.12	27.37	28.37	7	ZnS
76	0.08	0.21	0.10	0.47	0.12	25.10	26.08	7	ZnS
77	0.16	0.55	0.09	1.04	0.11	18.65	20.60	7	ZnS
78	0.11	0.10	0.09	0.17	0.73	100.00	101.20	7	CuFeS2
79	0.11	0.10	0.09	0.17	0.79	100.00	101.26	7	CuFeS2
80	0.11	0.10	0.09	0.17	0.86	261.99	263.32	7	CuFeS2
81	0.11	0.10	0.09	0.17	0.85	100.00	101.32	7	CuFeS2
82	0.10	0.10	0.09	0.17	0.88	100.00	101.34	7	CuFeS2
83	0.09	0.10	0.09	0.17	0.88	100.00	101.33	7	CuFeS2
84	0.08	0.10	0.09	0.17	0.82	100.00	101.26	7	CuFeS2
85	0.08	0.11	0.09	0.17	0.79	100.00	101.24	7	CuFeS2
86	0.07	0.11	0.09	0.17	0.71	100.00	101.15	7	CuFeS2
87	0.03	0.18	0.10	0.19	0.32	164.71	165.53	7	CuFeS2
88	0.03	0.45	0.10	0.17	1.01	100.00	101.76	7	InS
89	0.03	1.75	0.10	0.16	4.65	100.00	106.69	7	InS
90	0.03	0.65	0.10	0.16	1.15	100.00	102.09	7	InS
91	0.04	0.20	0.10	0.19	0.27	100.00	100.80	7	InS
92	86.50	0.74	0.10	5.18	0.10	53.80	146.42	Initial	ZnS
93	56.84	0.72	0.10	3.82	0.10	53.87	115.45	Initial	ZnS
94	171.08	0.70	0.10	5.49	0.10	21.48	198.95	Initial	ZnS

95	31.24	0.75	0.10	5.68	0.10	24.81	62.68	Initial	ZnS
96	100.00	0.70	0.10	14.58	0.10	100.00	215.48	Initial	ZnS
97	100.00	0.70	0.10	13.69	0.10	50.08	164.67	Initial	ZnS
98	100.00	0.74	0.10	16.44	0.10	28.77	146.15	Initial	ZnS
99	100.00	0.79	0.10	15.32	0.10	24.52	140.83	Initial	ZnS
100	100.00	0.80	0.10	13.75	0.10	25.41	140.16	Initial	ZnS
101	30.75	0.85	0.10	10.82	0.10	56.02	98.64	Initial	ZnS
102	6.61	0.12	0.10	0.13	3.70	100.00	110.66	Initial	CuFeS2
103	8.40	0.12	0.10	0.14	3.20	100.00	111.96	Initial	CuFeS2
104	5.66	0.11	0.09	0.14	3.44	100.00	109.44	Initial	CuFeS2
105	7.10	0.11	0.09	0.14	5.06	100.00	112.50	Initial	CuFeS2
106	7.60	0.11	0.09	0.14	3.79	100.00	111.73	Initial	CuFeS2
107	6.70	0.11	0.09	0.14	3.98	100.00	111.02	Initial	CuFeS2
108	6.46	0.11	0.09	0.14	5.30	100.00	112.10	Initial	CuFeS2
109	6.24	0.11	0.09	0.14	5.25	100.00	111.83	Initial	CuFeS2
110	9.61	0.11	0.09	0.14	7.80	100.00	117.75	Initial	CuFeS2
111	10.61	0.11	0.09	0.14	9.33	100.00	120.28	Initial	CuFeS2
112	5.98	0.11	0.09	0.14	3.72	100.00	110.04	Initial	CuFeS2
113	10.56	0.11	0.09	0.14	10.07	100.00	120.97	Initial	CuFeS2
114	9.94	0.11	0.09	0.14	8.25	100.00	118.53	Initial	CuFeS2
115	10.99	0.11	0.09	0.14	8.92	100.00	120.25	Initial	CuFeS2
116	17.20	0.11	0.09	0.14	9.73	100.00	127.27	Initial	CuFeS2
117	100.00	0.12	0.13	0.15	9.52	100.00	209.92	Initial	CuFeS2
149	34.77	0.11	0.09	0.14	8.33	100.00	143.44	Initial	CuFeS2
150	23.39	0.11	0.09	0.14	9.63	100.00	133.36	Initial	CuFeS2
151	17.64	0.11	0.09	0.14	9.50	100.00	127.48	Initial	CuFeS2
152	6.41	0.11	0.09	0.14	3.45	100.00	110.20	Initial	CuFeS2
153	9.63	0.11	0.10	0.13	3.28	100.00	113.25	Initial	CuFeS2
154	6.04	0.11	0.09	0.13	3.49	100.00	109.86	Initial	CuFeS2

Run product analyses (in weight percent) and starting sulfides followed by uncertainties due to counting statistics from experiments 8 - 11.

No.	In	Fe	S	Cu	Zn	Total	Run	Phase
1	2.760	34.404	35.185	25.186	3.068	100.60	8	CuFeS2
2	3.139	34.153	35.128	25.088	3.113	100.62	8	CuFeS2
3	3.728	33.495	34.684	24.882	3.407	100.20	8	CuFeS2
4	8.489	8.971	22.716	6.768	35.163	82.11	8	CuFeS2
5	6.999	9.476	18.012	7.066	37.969	79.52	8	CuFeS2
6	8.961	9.096	23.345	7.011	36.111	84.52	8	CuFeS2
7	0.362	35.600	34.399	24.339	2.872	97.57	8	CuFeS2
8	0.592	35.272	34.492	24.214	3.039	97.61	8	CuFeS2
9	0.741	35.076	34.199	23.990	3.114	97.12	8	CuFeS2
10	0.079	36.198	35.074	25.415	2.606	99.37	8	CuFeS2

11	0.146	36.337	34.992	25.626	2.737	99.84	8	CuFeS2
12	0.115	36.251	34.800	25.339	2.758	99.26	8	CuFeS2
13	0.016	35.737	34.271	23.910	2.587	96.52	8	CuFeS2
14	0.033	35.755	33.979	23.966	2.664	96.40	8	CuFeS2
15	0.050	35.712	34.238	23.907	2.711	96.62	8	CuFeS2
16	0.043	36.263	34.403	23.712	2.682	97.10	8	CuFeS2
17	b.d.l.	47.061	52.559	0.191	0.037	99.85	8	FeS
18	b.d.l.	46.949	52.735	0.130	0.000	99.82	8	FeS
19	b.d.l.	47.261	52.375	0.306	0.054	100.00	8	FeS
20	b.d.l.	47.182	52.672	0.159	0.026	100.04	8	FeS
21	b.d.l.	46.948	52.777	0.178	0.020	99.92	8	FeS
22	20.164	7.357	22.865	11.846	19.016	81.25	8	ZnS
23	28.562	7.738	28.839	15.823	16.586	97.55	8	ZnS
24	28.913	8.456	28.851	16.087	15.565	97.87	8	ZnS
25	21.118	9.312	28.459	12.495	24.163	95.55	8	ZnS
26	23.072	9.689	29.973	13.330	22.337	98.40	8	ZnS
27	30.274	7.846	27.975	16.699	13.655	96.45	8	ZnS
28	30.491	7.477	27.147	16.184	10.590	91.89	8	ZnS
29	32.852	5.862	26.171	17.876	10.241	93.00	8	ZnS
30	30.944	7.001	28.505	16.476	14.042	96.97	8	ZnS
31	30.289	7.098	28.787	16.013	15.000	97.19	8	ZnS
32	32.157	6.585	28.584	16.929	12.858	97.11	8	ZnS
33	32.732	6.378	28.370	17.300	11.864	96.64	8	ZnS
34	32.341	6.908	27.976	17.531	11.256	96.01	8	ZnS
35	28.059	8.136	28.723	15.811	15.815	96.54	8	ZnS
36	0.391	36.215	34.799	23.944	2.693	98.04	9	CuFeS2
37	0.452	36.192	34.614	24.152	2.747	98.16	9	CuFeS2
38	0.274	36.372	34.482	23.735	2.617	97.48	9	CuFeS2
39	0.263	36.280	34.690	23.714	2.630	97.58	9	CuFeS2
40	b.d.l.	47.315	52.693	0.059	b.d.l.	100.07	9	FeS
41	b.d.l.	47.433	52.685	0.044	b.d.l.	100.16	9	FeS
42	b.d.l.	47.400	52.693	0.042	b.d.l.	100.13	9	FeS
43	0.004	47.390	52.604	0.056	b.d.l.	100.05	9	FeS
44	3.765	33.042	33.846	23.239	3.781	97.67	9	CuFeS2
45	4.355	32.531	33.643	23.131	3.891	97.55	9	CuFeS2
46	5.610	31.647	33.752	22.962	4.158	98.13	9	CuFeS2
47	25.446	9.711	29.598	15.316	18.795	98.86	9	CuFeS2
48	23.524	10.128	30.242	14.461	21.124	99.48	9	CuFeS2
49	24.478	9.085	30.369	14.474	21.486	99.89	9	CuFeS2
50	28.660	8.522	28.547	16.674	14.684	97.09	9	CuFeS2
51	32.026	7.964	28.281	18.113	10.291	96.67	9	CuFeS2
52	5.296	28.326	30.871	18.565	2.627	85.69	9	CuFeS2
53	6.460	30.635	33.019	22.107	3.055	95.28	9	CuFeS2

54	6.497	30.577	32.895	22.026	3.156	95.15	9	CuFeS2
55	6.673	30.580	32.895	22.149	3.049	95.35	9	CuFeS2
56	19.888	18.924	30.652	19.343	7.064	95.87	9	CuFeS2
57	27.699	13.107	29.265	18.401	7.626	96.10	9	CuFeS2
58	45.477	0.163	26.103	23.236	0.209	95.19	9	CuFeS2
59	45.201	0.331	26.140	22.877	0.501	95.05	9	CuFeS2
60	45.752	0.231	26.216	23.030	0.171	95.40	9	CuFeS2
61	45.004	0.479	25.970	23.104	0.331	94.89	9	CuFeS2
62	44.679	0.266	26.132	22.603	0.262	93.94	9	CuFeS2
63	5.772	31.603	33.320	22.696	3.321	96.71	9	CuFeS2
64	7.018	30.706	32.864	22.327	3.042	95.96	9	CuFeS2
65	10.344	28.885	32.350	22.788	1.834	96.20	9	CuFeS2
66	40.533	3.694	26.289	22.644	1.758	94.92	9	CuFeS2
67	39.830	4.363	26.699	22.150	2.687	95.73	9	CuFeS2
68	4.109	32.187	33.459	22.380	4.141	96.28	9	CuFeS2
69	42.901	0.273	24.273	22.748	0.293	90.49	9	CuFeS2
70	45.862	0.065	25.833	23.451	0.108	95.32	9	CuFeS2
71	46.715	0.081	26.204	23.700	0.150	96.85	9	CuFeS2
72	46.224	0.091	25.712	23.628	0.193	95.85	9	CuFeS2
73	46.153	0.286	25.856	23.249	0.234	95.78	9	CuFeS2
74	b.d.l.	44.901	52.594	0.123	0.036	97.65	9	FeS
75	b.d.l.	45.025	51.865	0.122	b.d.l.	97.02	9	FeS
76	0.001	47.432	54.243	0.120	0.026	101.82	9	FeS
77	b.d.l.	47.387	52.955	0.096	0.022	100.46	9	FeS
78	0.004	46.563	52.735	0.254	0.045	99.60	9	FeS
79	b.d.l.	47.062	53.950	0.191	0.030	101.23	9	FeS
80	b.d.l.	46.152	52.348	0.020	0.030	98.55	10	FeS
81	b.d.l.	47.468	52.385	0.016	b.d.l.	99.87	10	FeS
82	b.d.l.	47.278	52.640	0.021	b.d.l.	99.95	10	FeS
83	b.d.l.	47.716	52.831	0.028	0.025	100.60	10	FeS
84	0.004	47.386	53.149	0.007	b.d.l.	100.55	10	FeS
85	b.d.l.	47.428	53.567	0.012	b.d.l.	101.01	10	FeS
86	6.293	31.875	33.998	24.659	3.853	100.68	10	CuFeS2
87	7.026	31.288	33.913	24.520	4.071	100.82	10	CuFeS2
88	7.067	31.427	34.021	24.493	4.114	101.12	10	CuFeS2
89	0.252	35.136	33.398	23.177	2.136	94.10	10	CuFeS2
90	0.307	35.142	33.548	22.963	2.189	94.15	10	CuFeS2
91	0.256	36.575	34.300	23.140	2.251	96.52	10	CuFeS2
92	0.756	35.371	34.221	24.785	2.774	97.91	10	CuFeS2
93	0.754	35.467	34.391	24.765	2.810	98.19	10	CuFeS2
94	0.719	35.468	34.376	24.768	2.784	98.11	10	CuFeS2
95	0.692	35.100	34.314	25.529	2.440	98.08	10	CuFeS2
96	0.727	36.291	34.951	25.347	2.565	99.88	10	CuFeS2

97	0.792	36.325	34.806	25.406	2.606	99.93	10	CuFeS2
98	b.d.l.	47.343	53.615	0.040	b.d.l.	101.00	10	FeS
99	b.d.l.	47.298	53.899	0.042	b.d.l.	101.24	10	FeS
100	b.d.l.	47.567	54.133	0.065	b.d.l.	101.77	10	FeS
101	15.330	10.687	30.930	9.779	32.513	99.24	10	ZnS
102	11.019	9.510	27.736	7.351	35.304	90.92	10	ZnS
103	13.481	10.673	31.397	8.823	34.578	98.95	10	ZnS
104	0.751	35.710	34.785	25.242	2.650	99.14	10	CuFeS2
105	0.684	35.819	34.720	25.282	2.636	99.14	10	CuFeS2
106	0.669	36.390	34.833	25.343	2.623	99.86	10	CuFeS2
107	0.004	45.887	51.727	0.107	b.d.l.	97.74	11	FeS
108	0.005	46.042	52.503	0.114	b.d.l.	98.66	11	FeS
109	b.d.l.	46.073	52.332	0.108	b.d.l.	98.53	11	FeS
110	1.743	33.974	34.109	22.592	3.112	95.53	11	FeS
111	1.776	34.824	35.214	22.710	3.230	97.75	11	FeS
112	0.795	35.669	34.465	23.747	3.108	97.78	11	CuFeS2
113	0.845	35.615	34.548	23.755	3.154	97.92	11	CuFeS2
114	0.812	35.753	34.326	23.619	3.148	97.66	11	CuFeS2
115	0.008	2.473	32.204	0.410	64.520	99.62	11	ZnS
116	0.008	2.856	33.171	0.385	64.067	100.49	11	ZnS
117	0.018	2.445	33.475	0.430	64.904	101.27	11	ZnS
118	1.665	34.953	34.149	23.248	3.616	97.63	11	ZnS
119	1.672	34.946	34.265	23.336	3.643	97.86	11	ZnS
120	1.711	34.913	34.159	23.157	3.606	97.54	11	ZnS
121	0.023	2.695	34.276	0.408	64.281	101.68	11	ZnS
122	0.014	2.389	30.347	0.399	63.813	96.96	11	ZnS
123	0.008	2.477	32.522	0.385	64.363	99.76	11	ZnS
124	0.228	36.008	34.409	23.792	2.821	97.26	11	CuFeS2
125	0.249	36.102	34.498	23.783	2.874	97.51	11	CuFeS2
126	0.290	36.257	34.681	23.769	2.834	97.83	11	CuFeS2
127	0.005	46.895	52.720	0.306	0.057	99.98	11	FeS
128	b.d.l.	47.118	52.309	0.291	0.045	99.76	11	FeS
129	b.d.l.	47.449	52.680	0.168	0.056	100.35	11	FeS
130	b.d.l.	47.357	53.338	0.169	0.031	100.90	11	FeS
131	0.005	47.130	52.847	0.176	0.048	100.21	11	FeS
132	1.180	35.078	33.684	22.890	3.173	96.01	11	FeS
133	1.180	35.123	33.643	23.162	3.245	96.35	11	CuFeS2
134	1.204	35.210	34.074	23.177	3.245	96.91	11	CuFeS2
135	0.001	0.003	32.990	b.d.l.	67.376	100.37	11	ZnS
136	b.d.l.	0.001	33.021	b.d.l.	67.690	100.71	11	ZnS
137	b.d.l.	b.d.l.	32.684	b.d.l.	67.831	100.51	11	ZnS
138	b.d.l.	59.081	38.199	0.093	b.d.l.	97.39	11	FeS
139	b.d.l.	59.167	38.544	0.073	b.d.l.	97.79	11	FeS

140	b.d.l.	59.074	38.764	0.098	b.d.l.	97.94	11	FeS
141	b.d.l.	30.465	34.520	33.462	0.038	98.48	11	CuFeS2
142	b.d.l.	30.612	34.436	33.554	0.033	98.64	11	CuFeS2
143	b.d.l.	30.617	34.429	33.365	0.043	98.45	11	CuFeS2
144	b.d.l.	30.660	34.346	33.374	0.021	98.40	11	CuFeS2
Relative Uncertainties (%)								
No.	**In**	**Fe**	**S**	**Cu**	**Zn**	**Total**	**Run**	**Phase**
1	0.41	0.15	0.09	0.17	0.61	1.43	8	CuFeS2
2	0.38	0.15	0.09	0.17	0.60	1.39	8	CuFeS2
3	0.34	0.15	0.09	0.18	0.57	1.33	8	CuFeS2
4	0.22	0.29	0.12	0.35	0.14	1.12	8	CuFeS2
5	0.24	0.28	0.13	0.35	0.14	1.14	8	CuFeS2
6	0.21	0.29	0.12	0.35	0.14	1.11	8	CuFeS2
7	1.60	0.15	0.09	0.18	0.63	2.65	8	CuFeS2
8	1.11	0.15	0.09	0.18	0.61	2.14	8	CuFeS2
9	0.94	0.15	0.09	0.18	0.60	1.96	8	CuFeS2
10	6.21	0.14	0.09	0.17	0.68	7.29	8	CuFeS2
11	3.50	0.14	0.09	0.17	0.66	4.56	8	CuFeS2
12	4.36	0.14	0.09	0.17	0.65	5.41	8	CuFeS2
13	28.86	0.15	0.09	0.18	0.67	29.95	8	CuFeS2
14	14.19	0.15	0.09	0.18	0.66	15.27	8	CuFeS2
15	9.22	0.15	0.09	0.18	0.66	10.30	8	CuFeS2
16	10.54	0.14	0.09	0.18	0.66	11.61	8	CuFeS2
17	430.77	0.13	0.07	5.40	28.84	465.21	8	CuFeS2
18	100.00	0.13	0.07	7.78	100.00	207.98	8	CuFeS2
19	100.00	0.13	0.07	3.51	19.60	123.31	8	CuFeS2
20	273.23	0.13	0.07	6.63	41.86	321.92	8	CuFeS2
21	100.00	0.13	0.07	5.88	54.01	160.09	8	CuFeS2
22	0.14	0.33	0.11	0.26	0.20	1.04	8	ZnS
23	0.11	0.32	0.10	0.22	0.22	0.97	8	ZnS
24	0.11	0.31	0.10	0.22	0.22	0.96	8	ZnS
25	0.13	0.29	0.10	0.25	0.18	0.95	8	ZnS
26	0.13	0.29	0.10	0.24	0.18	0.94	8	ZnS
27	0.11	0.32	0.10	0.21	0.24	0.98	8	ZnS
28	0.11	0.33	0.10	0.22	0.28	1.04	8	ZnS
29	0.11	0.38	0.11	0.21	0.28	1.09	8	ZnS
30	0.11	0.35	0.10	0.21	0.24	1.01	8	ZnS
31	0.11	0.34	0.10	0.22	0.23	1.00	8	ZnS
32	0.11	0.36	0.10	0.21	0.25	1.03	8	ZnS
33	0.11	0.36	0.10	0.21	0.26	1.04	8	ZnS
34	0.11	0.35	0.10	0.21	0.27	1.04	8	ZnS
35	0.12	0.32	0.10	0.22	0.22	0.98	8	ZnS
36	1.53	0.14	0.09	0.18	0.66	2.60	9	CuFeS2

37	1.36	0.14	0.09	0.18	0.66	2.43	9	CuFeS2
38	2.01	0.14	0.09	0.18	0.67	3.09	9	CuFeS2
39	2.11	0.14	0.09	0.18	0.67	3.19	9	CuFeS2
40	100.00	0.13	0.07	16.59	100.00	216.79	9	CuFeS2
41	100.00	0.13	0.07	22.69	100.00	222.89	9	CuFeS2
42	100.00	0.13	0.07	23.95	100.00	224.15	9	CuFeS2
43	123.24	0.13	0.07	17.51	100.00	240.95	9	CuFeS2
44	0.34	0.15	0.09	0.18	0.53	1.29	9	CuFeS2
45	0.31	0.15	0.09	0.18	0.52	1.25	9	CuFeS2
46	0.27	0.15	0.09	0.18	0.49	1.18	9	CuFeS2
47	0.12	0.29	0.10	0.22	0.20	0.93	9	CuFeS2
48	0.13	0.28	0.10	0.23	0.19	0.93	9	CuFeS2
49	0.12	0.30	0.10	0.23	0.19	0.94	9	CuFeS2
50	0.11	0.31	0.10	0.21	0.23	0.96	9	CuFeS2
51	0.11	0.32	0.10	0.20	0.28	1.01	9	CuFeS2
52	0.28	0.16	0.10	0.20	0.67	1.41	9	CuFeS2
53	0.25	0.16	0.09	0.19	0.60	1.29	9	CuFeS2
54	0.25	0.16	0.09	0.19	0.59	1.28	9	CuFeS2
55	0.25	0.16	0.09	0.18	0.60	1.28	9	CuFeS2
56	0.14	0.20	0.10	0.20	0.35	0.99	9	CuFeS2
57	0.12	0.25	0.10	0.20	0.34	1.01	9	CuFeS2
58	0.09	5.26	0.10	0.18	6.14	11.77	9	CuFeS2
59	0.09	2.85	0.10	0.18	2.70	5.92	9	CuFeS2
60	0.09	3.90	0.10	0.18	7.42	11.69	9	CuFeS2
61	0.09	2.03	0.10	0.18	3.92	6.32	9	CuFeS2
62	0.09	3.44	0.10	0.18	4.94	8.75	9	CuFeS2
63	0.27	0.15	0.09	0.18	0.57	1.26	9	CuFeS2
64	0.24	0.16	0.09	0.18	0.61	1.28	9	CuFeS2
65	0.19	0.16	0.09	0.18	0.87	1.49	9	CuFeS2
66	0.09	0.50	0.10	0.18	0.92	1.79	9	CuFeS2
67	0.10	0.45	0.10	0.18	0.67	1.50	9	CuFeS2
68	0.32	0.15	0.09	0.18	0.49	1.23	9	CuFeS2
69	0.09	3.35	0.11	0.18	4.47	8.20	9	CuFeS2
70	0.09	12.29	0.10	0.18	11.59	24.25	9	CuFeS2
71	0.09	10.40	0.10	0.17	8.44	19.20	9	CuFeS2
72	0.09	9.34	0.10	0.17	6.51	16.21	9	CuFeS2
73	0.09	3.19	0.10	0.18	5.48	9.04	9	CuFeS2
74	100.00	0.13	0.07	8.22	28.88	137.30	9	FeS
75	100.00	0.13	0.07	8.22	124.26	232.68	9	FeS
76	572.09	0.13	0.07	8.21	40.18	620.68	9	FeS
77	100.00	0.13	0.07	10.36	46.51	157.07	9	FeS
78	115.64	0.13	0.07	4.10	23.60	143.54	9	FeS
79	100.00	0.13	0.07	5.53	35.53	141.26	9	FeS

80	330.27	0.13	0.07	50.88	34.55	415.90	10	FeS
81	7880.92	0.13	0.07	61.38	100.00	8042.50	10	FeS
82	100.00	0.13	0.07	45.85	104.59	250.64	10	FeS
83	100.00	0.13	0.07	33.79	41.82	175.81	10	FeS
84	113.52	0.13	0.07	138.25	254.48	506.45	10	FeS
85	100.00	0.13	0.07	80.23	157.21	337.64	10	FeS
86	0.25	0.15	0.09	0.17	0.52	1.18	10	CuFeS2
87	0.24	0.16	0.09	0.17	0.50	1.16	10	CuFeS2
88	0.24	0.15	0.09	0.17	0.50	1.15	10	CuFeS2
89	2.15	0.15	0.09	0.18	0.77	3.34	10	CuFeS2
90	1.82	0.15	0.09	0.18	0.76	3.00	10	CuFeS2
91	2.12	0.14	0.09	0.18	0.75	3.28	10	CuFeS2
92	0.93	0.15	0.09	0.17	0.64	1.98	10	CuFeS2
93	0.93	0.15	0.09	0.17	0.63	1.97	10	CuFeS2
94	0.96	0.15	0.09	0.17	0.64	2.01	10	CuFeS2
95	0.99	0.15	0.09	0.17	0.70	2.10	10	CuFeS2
96	0.95	0.14	0.09	0.17	0.68	2.03	10	CuFeS2
97	0.90	0.14	0.09	0.17	0.67	1.97	10	CuFeS2
98	100.00	0.13	0.07	25.13	567.56	692.89	10	FeS
99	100.00	0.13	0.07	23.42	100.00	223.62	10	FeS
100	100.00	0.13	0.07	15.18	99.81	215.19	10	FeS
101	0.16	0.27	0.10	0.29	0.15	0.97	10	ZnS
102	0.19	0.28	0.10	0.34	0.14	1.05	10	ZnS
103	0.17	0.27	0.10	0.30	0.15	0.99	10	ZnS
104	0.94	0.14	0.09	0.17	0.66	2.00	10	CuFeS2
105	1.00	0.14	0.09	0.17	0.66	2.06	10	CuFeS2
106	1.02	0.14	0.09	0.17	0.66	2.08	10	CuFeS2
107	119.94	0.13	0.07	9.44	98.32	227.90	11	FeS
108	87.40	0.13	0.07	8.79	100.00	196.39	11	FeS
109	100.00	0.13	0.07	9.39	68.63	178.22	11	FeS
110	0.53	0.15	0.09	0.18	0.59	1.54	11	FeS
111	0.53	0.15	0.09	0.18	0.58	1.53	11	FeS
112	0.89	0.14	0.09	0.18	0.59	1.89	11	CuFeS2
113	0.85	0.14	0.09	0.18	0.59	1.85	11	CuFeS2
114	0.88	0.14	0.09	0.18	0.59	1.88	11	CuFeS2
115	58.34	0.59	0.10	2.78	0.10	61.91	11	ZnS
116	61.92	0.54	0.10	2.93	0.11	65.60	11	ZnS
117	26.19	0.60	0.10	2.66	0.10	29.65	11	ZnS
118	0.55	0.15	0.09	0.18	0.54	1.51	11	ZnS
119	0.54	0.15	0.09	0.18	0.53	1.49	11	ZnS
120	0.54	0.15	0.09	0.18	0.54	1.50	11	ZnS
121	20.97	0.56	0.10	2.85	0.11	24.59	11	ZnS
122	32.17	0.60	0.10	2.89	0.11	35.87	11	ZnS

123	63.41	0.59	0.10	2.97	0.10	67.17	11	ZnS
124	2.35	0.14	0.09	0.18	0.64	3.40	11	CuFeS2
125	2.16	0.14	0.09	0.18	0.62	3.19	11	CuFeS2
126	1.92	0.14	0.09	0.18	0.63	2.96	11	CuFeS2
127	91.38	0.13	0.07	3.46	18.53	113.57	11	FeS
128	100.00	0.13	0.07	3.64	23.83	127.67	11	FeS
129	100.00	0.13	0.07	6.10	19.01	125.31	11	FeS
130	100.00	0.13	0.07	5.99	34.04	140.23	11	FeS
131	82.36	0.13	0.07	5.96	22.15	110.67	11	FeS
132	0.68	0.15	0.09	0.18	0.59	1.69	11	FeS
133	0.68	0.15	0.09	0.18	0.58	1.68	11	CuFeS2
134	0.67	0.15	0.09	0.18	0.58	1.67	11	CuFeS2
135	665.05	207.57	0.10	100.00	0.10	972.82	11	ZnS
136	100.00	681.14	0.10	100.00	0.10	881.34	11	ZnS
137	100.00	100.00	0.10	100.00	0.10	300.20	11	ZnS
138	100.00	0.11	0.08	10.70	63.40	174.29	11	FeS
139	100.00	0.11	0.08	13.94	296.51	410.64	11	FeS
140	100.00	0.11	0.08	10.16	100.00	210.35	11	FeS
141	100.00	0.16	0.09	0.15	28.89	129.29	11	CuFeS2
142	409.38	0.16	0.09	0.15	34.13	443.91	11	CuFeS2
143	100.00	0.16	0.09	0.15	25.53	125.93	11	CuFeS2
144	100.00	0.16	0.09	0.15	51.80	152.20	11	CuFeS2

Honor Pledge:
I pledge on my honor that I have not given nor received any unauthorized assistance on this assignment.

_____